Universidade de Aveiro
Ano 2021

João Maria Silva Pinto Leite

Nanopartículas multifuncionais de celulose para potencial aplicação no diagnóstico e tratamento de cancro

Multifunctional cellulose nanoparticles for potential application on the diagnosis and treatment of cancer

Universidade de Aveiro
Ano 2021

João Maria Silva Pinto Leite

Nanopartículas multifuncionais de celulose para potencial aplicação no diagnóstico e tratamento de cancro

Multifunctional cellulose nanoparticles for potential application on the diagnosis and treatment of cancer

Dissertação apresentada à Universidade de Aveiro para cumprimento dos requisitos necessários à obtenção do grau de Mestre em Materiais e Dispositivos Biomédicos, realizada sob a orientação científica da Doutora Carla Andreia Cunha Vilela, Investigadora Auxiliar do Departamento de Química da Universidade de Aveiro e da Doutora Carmen Sofia da Rocha Freire, Investigadora Principal com Agregação do Departamento de Química da Universidade de Aveiro

Dedico esta tese aos meus pais, ao meu irmão e a todos os meus amigos que sempre me apoiaram ao longo do meu percurso.

o júri

presidente

Professor Doutor João André da Costa Tedim
Professor Auxiliar da Universidade de Aveiro

Doutora Helena Cristina Correia de Oliveira
Investigadora Auxiliar da Universidade de Aveiro

Doutora Carla Andreia Cunha Vilela
Investigadora Auxiliar da Universidade de Aveiro

agradecimentos

Gostaria de agradecer à minha orientadora, Doutora Carla Vilela, por me ter dado a oportunidade de desenvolver este trabalho, pela sua constante disponibilidade, excelente orientação científica e incansável apoio prestado no decorrer desta dissertação.

Agradeço também à minha coorientadora, Doutora Carmen Freire, pela sua disponibilidade, motivação, correções, e acompanhamento ao longo deste trabalho, sem o qual este teria sido muito mais custoso.

Agradeço a todos os meus colegas e amigos do laboratório por proporcionarem um bom ambiente e pela sua permanente disponibilidade.

À Ana Cristina Silva, o meu profundo agradecimento pela sua paciência, boa disposição, disponibilidade e imensurável orientação, nos aspetos práticos e teóricos do trabalho laboratorial.

Gostaria de agradecer também ao Doutor Ricardo Pinto pelas análises de microscopia eletrónica, e à Doutora Verónica Bastos e à Doutora Helena Oliveira pela realização dos ensaios de viabilidade celular.

Agradeço também a todos os membros do Complexo de Laboratórios Tecnológicos da Universidade de Aveiro pelo seu apoio e contribuição para a minha aprendizagem e manuseamento dos diversos equipamentos para realizar o meu trabalho.

Por fim, gostaria de agradecer à minha mãe, ao meu pai, ao meu irmão e à minha melhor amiga, pela indispensável motivação, apoio e bem-estar que proporcionaram ao longo deste percurso, sem o qual não seria possível chegar onde estou hoje.

palavras-chave

Acetato de celulose, nanoprecipitação, nanobeads de celulose funcionalizadas, nanopartículas de ouro, diagnóstico e terapia de cancro

resumo

Nanobeads biopoliméricas destacam-se como sendo nanomateriais biocompatíveis, biodegradáveis e quimicamente versáteis para diversas aplicações biomédicas. Neste âmbito, a celulose tem demonstrado um potencial crescente para estas aplicações devido à sua abundância de grupos hidroxilo e consequente aptidão para ser funcionalizada. Neste contexto, o objetivo da presente dissertação consiste na preparação e caracterização de nanobeads multifuncionais à base de celulose para potencial aplicação no diagnóstico e tratamento do cancro.

Nanobeads esféricas à base de celulose foram produzidas por nanoprecipitação e funcionalizadas com nanopartículas de ouro (AuNPs) que podem desempenhar um papel duplo como agente de contraste para imagiologia e agente terapêutico. As nanobeads de celulose foram preparadas usando acetato de celulose (CA) como matéria-prima inicial em vez de usar diretamente a celulose devido à sua insolubilidade na maioria dos solventes convencionais. Deste modo, as nanobeads de CA foram obtidas por nanoprecipitação através da dissolução e regeneração do CA, seguida de uma hidrólise alcalina para a obtenção das nanobeads de celulose. Posteriormente, desenvolveram-se sistemas híbridos de nanobeads de celulose/AuNPs seguindo duas metodologias distintas, nomeadamente, por regeneração de CA na presença de AuNPs e subsequente hidrólise alcalina, ou pela redução *in situ* do sal de ouro na presença das nanobeads de celulose. Os sistemas híbridos foram posteriormente caracterizados por microscopia eletrónica de varrimento (SEM), microscopia eletrónica de varrimento em modo de transmissão (STEM), espectroscopia de infravermelho com reflexão total atenuada e transformada de Fourier (ATR-FTIR), e espectroscopia de ultravioleta-visível (UV-vis).

Em suma, a produção de nanobeads de celulose foi conseguida dissolvendo o CA em acetona e subsequente regeneração usando água como o anti-solvente, seguida de hidrólise alcalina. O sucesso da hidrólise foi comprovado por espectroscopia de ATR-FTIR e SEM, enquanto que a síntese das AuNPs foi confirmada por espectroscopia de UV-vis e STEM. A morfologia e o tamanho dos sistemas híbridos foram avaliados por SEM e STEM, os quais confirmaram a produção de sistemas híbridos de nanobeads de celulose/AuNPs com tamanho médio de 415±187 nm para as nanobeads de celulose e 15±3 nm para as AuNPs. Adicionalmente, a citotoxicidade *in vitro* dos sistemas híbridos foi avaliada em células humanas pigmentadas de melanoma (MNT-1) ao fim de 24 h. Os resultados mostraram que o sistema híbrido possui uma toxicidade celular dependente da concentração, alcançando 81.6±4.5% de viabilidade celular para 39.0 μg mL^{-1} do híbrido. Deste modo, uma concentração mais elevada promoverá uma maior resposta citotóxica nas células cancerígenas. Todos os resultados obtidos evidenciam o potencial dos sistemas híbridos de nanobeads de celulose/AuNPs para aplicação no diagnóstico e terapia do cancro.

keywords

Cellulose acetate, nanoprecipitation, functional cellulose nanobeads, gold nanoparticles, cancer therapy and diagnostics

abstract

Biopolymeric nanobeads stand out as being biocompatible, biodegradable, and chemically versatile nanomaterials for several biomedical applications. In this context, cellulose has shown an increasing potential in this field due to its abundance of hydroxyl groups and consequent ability to be functionalized. Therefore, the objective of the present dissertation consists in the preparation and characterization of multifunctional cellulose-based nanobeads for potential application in cancer diagnosis and treatment.

Spherical cellulose-based nanobeads were produced by nanoprecipitation and functionalized with gold nanoparticles (AuNPs) that will play the dual role of cell imaging and therapeutic agent. The cellulose nanobeads were prepared using cellulose acetate (CA) as the starting raw material instead of directly using cellulose because of its high insolubility in most common solvents. So, CA nanobeads were obtained by nanoprecipitation through CA dissolution and regeneration, followed by alkaline hydrolysis to obtain the cellulose nanobeads. Subsequently, cellulose nanobeads/AuNPs hybrid systems were developed by two distinct methodologies, namely by CA regeneration in the presence of AuNPs and subsequent alkaline hydrolysis, or by the *in situ* reduction of the gold salt in the presence of the cellulose nanobeads. The cellulose nanobeads/AuNPs hybrids were then characterized by scanning electron microscopy (SEM), scanning transmission electron microscopy (STEM), attenuated total reflection-Fourier transform infrared (ATR-FTIR) spectroscopy, and ultraviolet-visible spectroscopy (UV-vis).

Overall, the production of the cellulose nanobeads was achieved by dissolving CA in acetone and subsequent regeneration using water as the non-solvent, followed by alkaline hydrolysis. The success of the hydrolysis was confirmed by ATR-FTIR spectroscopy and SEM, while the synthesis of AuNPs was corroborated by UV-vis spectroscopy and STEM. The morphology and size of the hybrid systems were evaluated by SEM and STEM, which confirmed the production of the cellulose nanobeads/AuNPs hybrids with an average size of 415±187 nm for the cellulose nanobeads and 15±3 nm for the AuNPs. Moreover, the *in vitro* cytotoxicity of the cellulose nanobeads/AuNPs hybrids towards the pigmented human melanoma (MNT-1) cell line was evaluated for 24 h. The resultant data showed that the hybrid system exhibits a dose-dependent cellular toxicity, reaching 81.6±4.5% of cell viability for 39.0 μg mL^{-1} of hybrid system. Thus, a higher dose will most definitely translate into a higher cytotoxic effect towards the tumor cells. All the obtained results revealed that the cellulose nanobeads/AuNPs hybrids have potential for application in the diagnosis and therapy of cancer.

Contents

List of Abbreviations

ATR-FTIR	Attenuated total reflection-Fourier transform infrared spectroscopy
AuNPs	Gold nanoparticles
CA	Cellulose acetate
CNCs	Cellulose nanocrystals
CNFs	Cellulose nanofibers
CP/MAS	Cross Polarization-Magic angle spinning
CT	Computed tomography
DMSO	Dimethyl sulfoxide
DP	Degree of polymerization
EPR	Enhanced permeability and retention
MNT-1	Pigmented human melanoma cell line
MRI	Magnetic resonance imaging
NMMO	*N*-methylmorpholine oxide
NMR	Nuclear magnetic resonance
NPs	Nanoparticles
PEG	Poly(ethylene glycol)
PET	Positron emission tomography
RES	Reticuloendothelial system
SEM	Scanning electron microscopy
SPECT	Single photon emission computed tomography
SPR	Surface plasmon resonance
STEM	Transmission scanning electron microscopy
TBAF	Tetrabutylammonium fluoride
UV-vis	Ultraviolet-visible spectroscopy

List of Figures

List of Tables

THE CONTEXT

To this days, cancer remains a menacing reality, with more than 10 million new cases every year.[1,2] The drawbacks of conventional treatment modalities, such as the non-specific distribution of anti-cancer drugs throughout the body and the development of multi-drug resistance, request more efficient and safe alternatives. One such alternative is targeted drug delivery.[3,4] For example, this concept exploits nanosized materials for tumor targeting, diagnosis, and therapy. Specific targeting allows a more precise delivery of drugs to tumor sites while reducing possible adverse effects, and for this purpose, there are a plethora of nanoparticles with tunable properties, that are dependent on size, materials composition, surface charge, and shape.[3]

Biopolymers possess unique properties suitable for the development of drug delivery systems owing to their physicochemical versatility, cost-effectiveness, biocompatibility, biodegradability, and reduced immunogenicity.[5,6] In this regard, cellulose is the most widely available biopolymer in the world and possesses promising properties, including biocompatibility, renewability, and potential for chemical modification, making it a suitable material for developing nanosystems for drug delivery.[7]

In this context, the present dissertation aims to develop cellulose nanobeads functionalized with gold nanoparticles, for potential application in cancer imaging and therapy. Herein, this dissertation is organized into four chapters, namely bibliography review, experimental part, results and discussion, and conclusions and future work. In the first chapter (Chapter 1), a bibliographic appraisal of the status of cancer therapy, and the fundamental aspects of cellulose as a promising drug delivery agent, is presented. The second chapter (Chapter 2) describes the chemicals and materials, as well as the most relevant experimental methods and characterization techniques used in this work. The third chapter (Chapter 3) presents the results and their discussion and comparison with literature. Lastly, the fourth chapter (Chapter 4) presents the main conclusions obtained in this research, as well as the discussion of some lines to future work.

CHAPTER 1 – BIBLIOGRAPHY REVIEW

1.1. The status of cancer therapy

Cancer remains to these days one of the deadliest diseases, with millions of people being diagnosed each year. In fact, the World Health Organization projects that the number of deaths caused by cancer will increase up to ~13.1 million by the year 2030.[2] Cancer can be described as a group of diseases that consist on the uncontrolled proliferation of malignant cells, which may spread to other body parts.[1,2,8] In the latter decades, huge efforts and resources have been invested on the detection, treatment, and cure of this disease. However, due to the complexity, diversity and heterogeneity of tumors, the success of current treatment options is limited, boosting the search for more effective and safe alternatives.[9] In the next sections, a brief review of current clinical cancer treatments will be presented, culminating on the recent contributions of nanotechnology and drug delivery to this realm.

1.1.1. Conventional cancer therapeutics

Cancer therapy can be ruled by a quote from General George S. Patton: "A good battle plan that you act on today can be better than a perfect one tomorrow," where the detection of the disease at the earliest stages, or even at its pre-malignant form, can greatly increase the chances of a successful treatment.[9–11]

In the later decades, cancer diagnosis has improved significantly due to the fast development of medical imaging techniques, namely, magnetic resonance imaging[10] (MRI), ultrasound[12], photoacoustic imaging[13], fluorescence imaging[14], computed tomography (CT) imaging[15], positron emission tomography[16] (PET) and single photon emission computed tomography[17] (SPECT). However, most of these techniques can only detect cancer based on a noticeable change in the tissue, which by then, many cancer cells may have already proliferated or metastasized. Moreover, distinguishing between benign and malignant lesions is not possible with current imaging methods.[11] Despite the advances in imaging modalities and their contribution to cancer research and patient care, targeted imaging techniques that are able to evaluate changes at the molecular level *in vivo* are still urgently needed.[18] In ideal circumstances, the sensitivity

of diagnostic methods should allow the detection of microscopic changes at molecular level while bearing sufficient specificity to discern between disease stages.[9]

Regarding the current cancer therapies, chemotherapy, radiotherapy, surgery, and high intensity focused ultrasound have proven successful in suppressing tumors proliferation and extending the patient's survival.[9,19] However, these may bear the disadvantage of not only affecting the tumor tissues, but healthy tissues as well. Chemotherapy, for example, relies on the use of drugs such as doxorubicin, paclitaxel, or docetaxel to eradicate tumors.[9] Although its intake by tumors results in rapid killing of tumor cells, its rapid clearance and non-specific distribution hinder its effectiveness, and due the potency of modern pharmacological drugs, and the fact that the dose obtained within solid tumors is limited, excessive systemic toxicities are often a harmful consequence.[9,20]

To conclude, there are still great obstacles to be overcome regarding the treatment of cancer, whether in diagnostics or therapeutics. In the first, clinically applicable probes or contrast agents, and the cost-effective employment of highly sensitive technologies that allow the detection of cancer at early stages are still a challenge.[10,11] As for the latter, low specificity, rapid drug clearance, systemic toxicity and ineffective targeting constitute the major challenges in the area.[19,20] In view of the current drawbacks of cancer therapeutics, nanotechnology is an emerging field that has contributed significantly to increase the efficacy and safety of cancer treatments in the last two decades.[21,22] It has captured the interest of the scientific community, aiming to use nanostructured systems for cancer therapy, as evidenced in Figure 1 by the increasing number of nanotechnology-related publications over the years.[23]

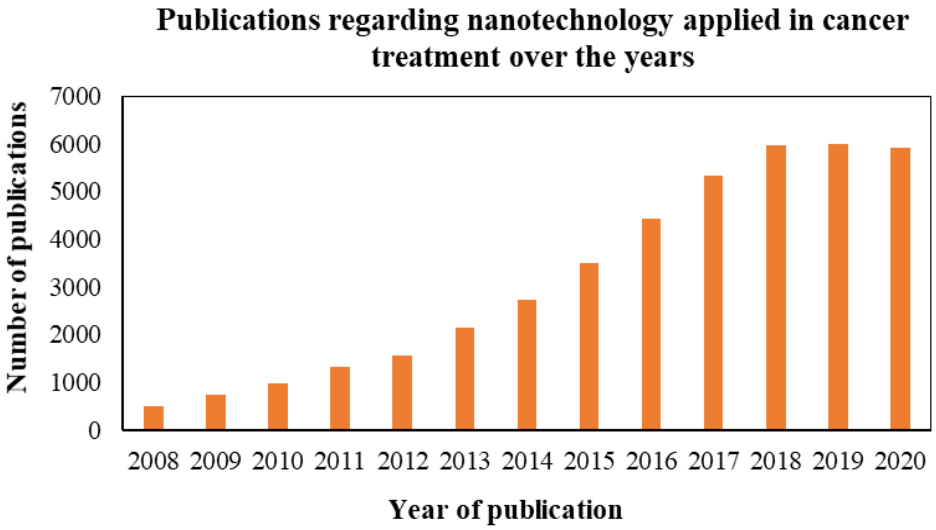

***Figure 1**. Number of publications referring to nanotechnology applied in cancer treatment over the years, retrieved from Web of Science using the following keywords: nanotechnology, nanoparticle, cancer treatment, and cancer therapy. Accessed in December 2020.*

1.1.2. **Nanotechnology's contribution to cancer treatment**

Nanotechnology is a multidisciplinary field that consists on the engineering and manufacturing of structures up to several hundreds of nanometers, produced by either top-down or bottom-up approaches from a single component.[24,25].[25] The application of nanotechnology in cancer treatment has bolstered diagnosis and imaging techniques to a new level, improved the development of synthetic vaccines and miniaturized devices, and has increased the therapeutic potential of several materials.[22] In truth, nanotechnology aims to tackle several aspects of cancer therapy, namely, solubility of poorly soluble drugs, specificity of targeted drug delivery, transcytosis of drugs across epithelial and endothelial barriers, intracellular delivery of large macromolecules, co-delivery of two or more therapeutic agents for combined therapy, imaging modalities, and real time assessment of the *in vivo* effectiveness of a drug.[25] In regards to cancer diagnostics, it opens new doors by applying nano-scaled devices that are able to operate at smaller scales where biological or physiological processes occur. However, *in vivo* diagnostics based on nanomaterials is still in early development due to unknown toxic effect, clearance mechanisms, and disease-targeting capabilities.[10,11]

In respect to treatment options, nanotechnology is also substantially contributing to several recent treatment alternatives, such as photothermal therapy[9],

immunotherapy[26], gene therapy[3], and magnetic hyperthermia[27], that have demonstrated increasing treatment efficacy and reducing potential side effects.[9] These techniques have proven to be highly efficient cancer treatments in laboratorial tests and pre-clinical research and showing great expectations for the near future. Nevertheless, when treating cancer, a single treatment modality is generally not able to completely eliminate a tumor, neither to prevent metastasis.[9,28] The main reason for this is that the heterogenous tumor tissues may possess subpopulations of cancer cells that are able to resist monotherapy.[9] An example of such occurrence lies in the long-term use of anticancer drugs, which induces multidrug resistance.[29,30] Thus, in order to surpass this obstacle, combined therapies, which integrates two or more distinct forms of treatment, are preferred. In fact, cancer therapy has been increasingly shifting from monotherapy to combined therapy, more specifically multimodal synergistic therapy.[9] It integrates different treatments into a single nanoplatform, resulting in better therapeutic outcomes than the simple combination of the individual treatments.[31] This approach carries multiple advantages in comparison to its monotherapy counterparts. For example, because of the synergistic effects, it requires a lower dosage to achieve a higher anticancer efficacy, therefore avoiding the side effects induced by high dosages.[9] To this end, drug delivery stands out, making use of nanoparticles (NPs) ranging from 1 to 1000 nm, to bring anticancer therapeutic agents to tumor cells.[21] A well designed NP can serve as an excellent carrier of more than one active molecular or macromolecular agent, which can be incorporated within their bulk, within its pore network, or even attached to its surface, serving as ideal platforms to deliver multimodal synergistic therapies.[9,24]

1.1.3. **Drug delivery**

The inspiration for the use of NPs on drug delivery applications comes from our own bodies, where natural NPs exist, namely lipids, proteins, and other complex biomacromolecules that act as normal body function regulators or as carriers for active molecules. The latter originated the term “nanocarrier” where, as the name says, its function is to carry a specific load, usually a drug, to a specific site.[1] NPs can present various shapes, such as spheres, rods, wires, planes, stars, cages, multipods, among others.[32] Depending on the material and assembly strategy, NPs can possess several unique characteristics when compared to their bulk counterparts, namely, high surface

energy, high surface-to-volume ratio, unique mechanical, thermal, electrical, magnetic, and optical behaviors. In addition, surface modifications of NPs with specific functional groups can improve their chemical reactivity and dispersibility in various solvents, according to the desired applications.[32,33] Simply put, the general principle in the use of NPs is to efficiently carry and deliver imaging probes[34], therapeutic agents[19,35], or biological materials[8] to a specific target, such as an organ, tissue, or even an underlying cell. In fact, the earliest examples of the application of nanotechnology in medicine consisted of drug loaded lipid- and polymer-based nanocarriers for targeted sustained drug delivery.[36] In addition, they can also possess active functions that make them suitable for their use as nanoprobes with applications in imaging and sensing.[1,24,32] Thus, these materials are well suited for drug delivery applications, however, the manner in which they are assembled is very important to ensure the desired outcomes. For this, NPs are usually multifunctional nanosystems, exhibiting several components that play its assigned role. Figure 2 exhibits some examples of the functionalities exhibited by multifunctional NPs.[24]

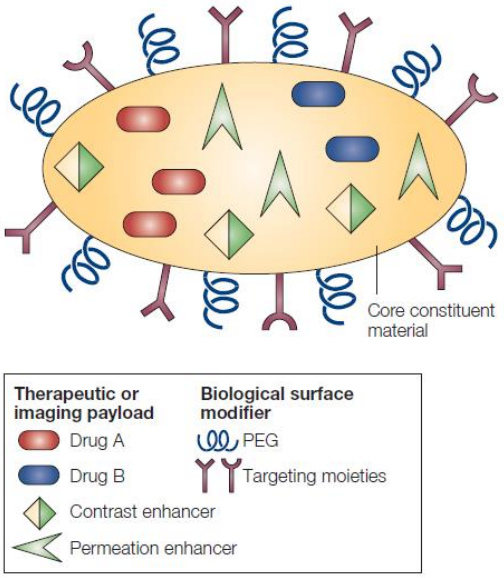

Figure 2. *Example of a multifunctional nanoparticle. Image reprinted from reference [24].*

As shown, one NP can carry more than one type of drug, assembling multiple therapeutic agents into a single nanostructure using physical adsorption or chemical binding, with view to apply a multimodal synergistic therapy.[9,20] In addition, functionalization enables the biomolecular targeting of one or more conjugated antibodies, while carrying contrast enhancers to allow clean imaging signal

amplification.[37] Moreover, permeation enhancers can be added to facilitate the access to target cells, and poly(ethylene glycol) (PEG) is commonly used to avoid the uptake of NPs by macrophages. NPs can be tailored in terms of composition, size, shape, and surface properties in order to protect the loaded drugs from degradation by several endogenous defense mechanisms.[38] Most of these defenses consist in enzymatic degradation, immunodegradation, capture by the reticuloendothelial system (RES) in the bloodstream, acid hydrolysis in the stomach and mucociliary clearance in the lungs.[1] The ability to control their morphological aspects and surface properties results in the accurate targeting of not only specific organs and tissues in the body, but also specific cellular and subcellular entities. Furthermore, the development of nanocarrier matrices allow a controlled release of drugs at their targets, ensuring optimal and sustained drug action.[32] Generally, there are two approaches for target drug delivery, namely, passive and active targeting. Passive targeting relies in the increased permeability of leaky tumor vasculature (pores up to 1 μm in size), also known as the enhanced permeability and retention (EPR) effect, for extravasation of NPs from the blood stream to the tumor itself, as depicted in Figure 3.[1,3,19,39]

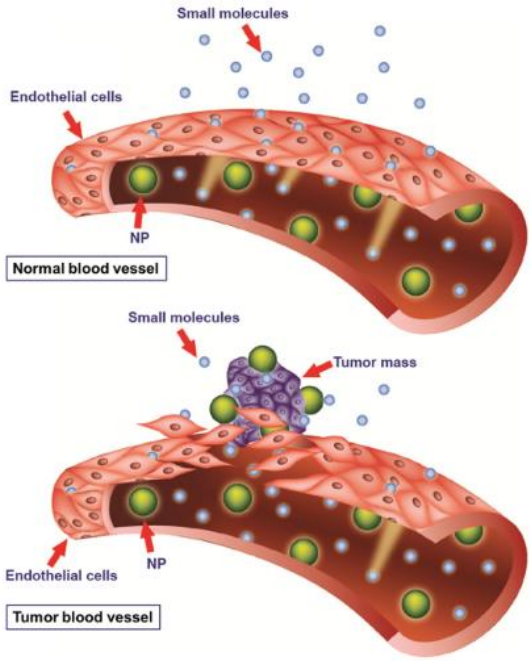

***Figure 3**. Drug delivery via the EPR effect. Normal blood vessels are made of tightly connected endothelial cells which hinder the diffusion of NPs through them. Tumor blood vessels exhibit large fenestrations between endothelial cells, permitting NPs to reach the tumor cells. Reprinted from reference [39].*

It can be said that passive targeting depends on the pathophysiological properties of the tumor (temperature, pH, and surface charge of tumor cells) and therefore may suffer from lack of EPR effect in some cases, as well as inefficient drug diffusion.[3,19] In addition, passive targeting excludes the possibility of NPs diffusing into tissues who possess naturally fenestrated blood vessels, such as the liver or the spleen.[19] Active targeting, on the other hand, resolves this matter by adding ligands, with binding affinity to specific tumor biomarkers, to the NPs, enhancing the interactions between the NPs and the tumor. In other words, the surface of these materials can be modified with proteins, peptides, or other biomolecules to specifically bind to overexpressed receptors present in the tumor cells and also to prevent non-specific uptake by the reticuloendothelial system.[1,3,19] The principle of active targeting is illustrated in Figure 4. Also, lymphatic vessels, which are used to transport solutes into circulation, are impaired in tumor sites. Therefore, macromolecules with more than 4 nm in size are usually retained.[20,39]

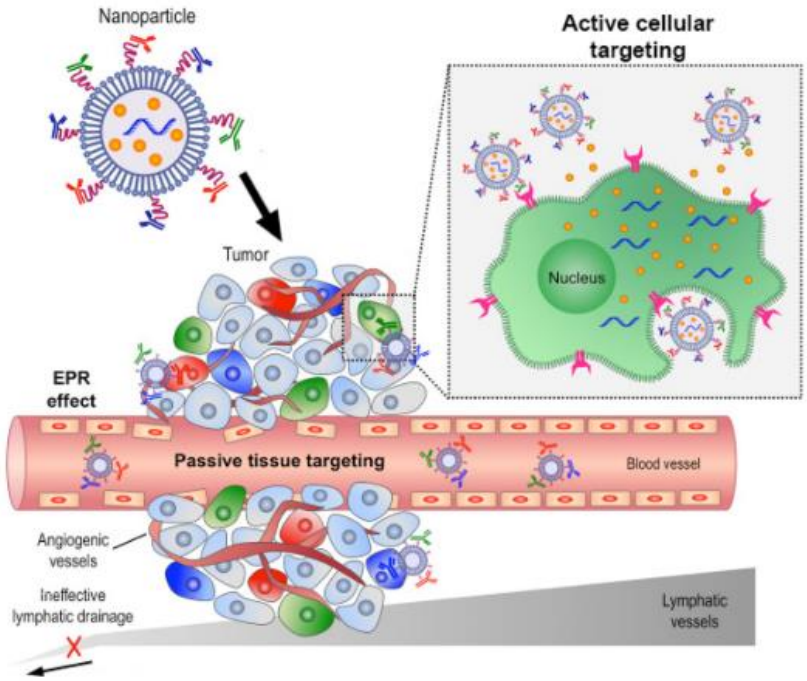

***Figure 4**. Active targeting mechanism in drug delivery via nanoparticles. The NPs circulate through blood vessels until diffusion by the EPR effect, after which cellular receptors are recognized enabling cell internalization. Reprinted from reference [39].*

Furthermore, stimuli-responsive systems may be employed to trigger the release of drugs according to internal or external stimuli.[36] Internal stimuli consist of changes in

pH, oxidation and reduction of compounds, ionic strength and stress in the targeted tissue, while external stimuli consist of temperature, light, ultrasound, magnetic force and electric fields.[19,40] Nowadays, there are a plethora of drug delivery nanoplatforms that can be classified according to composition, structure, and properties, as summarized in Figure 5, along with the advantages and disadvantages of each class.[41]

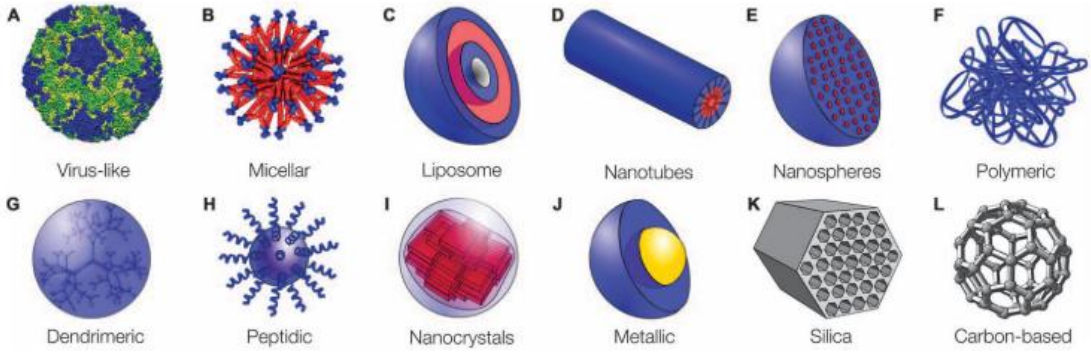

Nanoparticle	Advantages	Disadvantages
Virus	High efficiency	Trigger immune response Poor drug-loading capacity
Micellar	Efficient loading of hydrophobic drugs Excellent cell penetration	Poor stability Liver accumulation Cytotoxic
Polymeric	Excellent functionalization High versatility	Polydisperse Cytotoxic
Dendrimers	Facilitate endosomal escape Controllable generation Easy functionalization	Cytotoxic
Peptidic	Increased cell penetration High specificity	Poor stability Self-aggregation
Nanocrystals	High loading capacity Good dissolution	Limited applicability
Metallic	Tunable shape and size	Cytotoxic Not biodegradable
Sillica	High loading capacity Easy functionalization Good biocompatibility	Poor solubility
Carbon-based	Stable Good cell penetration Tunable size and shape	Cytotoxic Immune suppressors Poor reactivity

***Figure 5**. Different types of nanoparticles and their respective advantages and disadvantages. Adapted from reference [41].*

In this regard, NPs made of bio-based polymers, also known as biopolymers, show great potential for drug delivery applications due to their excellent biodegradability, biocompatibility, ease of processing, and versatility.[6,42,43] Commonly used biopolymers for said applications include alginate, chitosan, collagen, gelatin, silk,

and cellulose, among others.[6,43–45] Some examples are provided in Figure 6, along with their chemical structures. Alginate for example, is a natural polysaccharide retrieved from brown algae and it is known for its gel-forming properties achieved by the addition of divalent cations.[46] In fact, alginate-based gels are characterized by their water retention capabilities, tunable chemical and mechanical properties, and muco-adhesive behavior, making it a great candidate for the sustained and targeted release of drugs.[6,45,46]

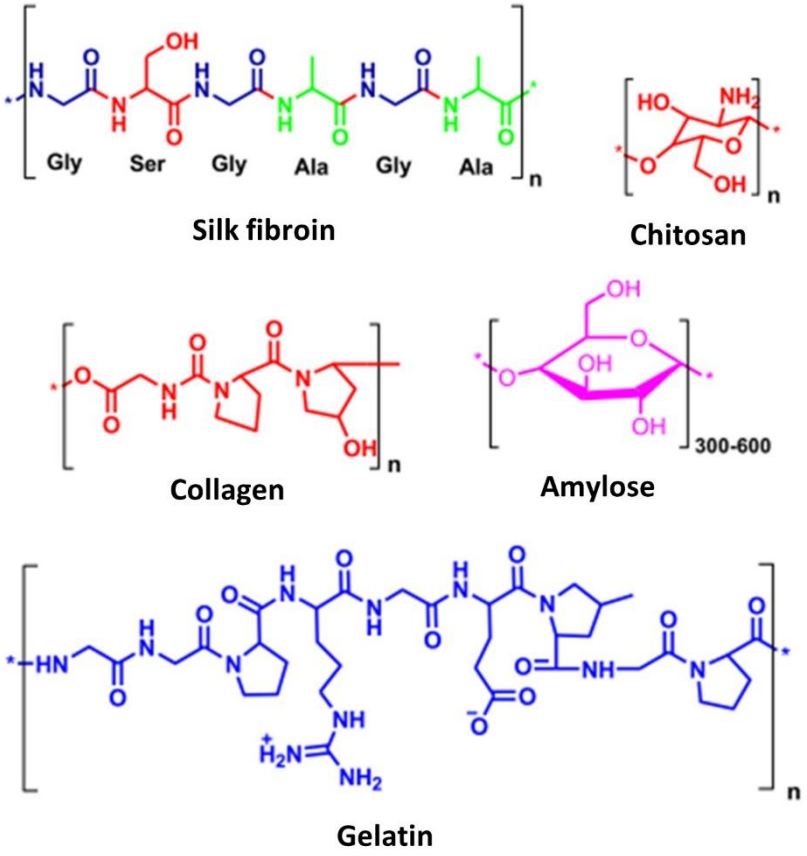

***Figure 6**. Chemical structures of biopolymers with applications in drug delivery.*[45]

In a practical approach, Ayub *et al.*[35] developed biocompatible disulphide cross-linked sodium alginate based NPs, for targeted delivery of paclitaxel to treat colon cancer. Silk fibroin proteins consist of natural fibers with potential for several therapeutic applications. Its innate mechanical hardness, versatile processing, and self-assembly have allowed its use in the development of hydrogels, electrospun fibers, films, and three-dimensional scaffolds.[45] As reported by Seib *et al.*,[47] silk fibroin NPs exhibited a pH-dependent drug release. Briefly, the loss of the negative net charges at

pH 4.5 is responsible for weakening the electrostatic interaction between silk fibroin molecules and the drug DOX, thus accelerating its release from the NPs.[47,48] Chitosan for example, is the second most abundant biopolymer and is known for its non-toxicity, anti-bacterial, biodegradability, and versatility due to its active amino (NH_2) and hydroxyl (OH) groups which serve as attachment sites for the attachment of new groups.[49] Several chitosan-based systems have been developed, namely, microspheres, tablets, nanoparticles, and nanofibers, among others.[49] For example, Barbieri *et al.*[50] prepared lecithin-chitosan NPs loaded with tamoxifen, an anti-cancer drug with poor water solubility. This system revealed an increased drug permeation across the intestinal epithelium, which consequently improves the drug's bioavailability and its anti-estrogenic effect purposed for estrogen-dependent breast cancer.[50]

Similarly, cellulose, which possesses a chemical structure intimately related to chitosan, is the most abundant biopolymer in the world, and is sought out due to its innate availability of hydroxyl groups and biocompatibility, and being the main focus of this work, it will be discussed in detail in the following paragraphs.[51]

1.2. Cellulose as a promising drug delivery agent

Cellulose and its derivatives have been widely used throughout the years in the most basic applications, such as the production of paper and textiles. In this regard, cellulose comes forth as an organic raw material that has earned its appeal for being biodegradable, biocompatible, renewable and because of its unique physicochemical properties.[52] With an annual production of over 7.5×10^{10} tons, it is the most abundant biopolymer in the planet, and can be found naturally in plants, animals, and fungi although its major source are plant fibers, where cellulose acts as a structural component in the cell walls.[53,54]

Developments in science and technology allowed to get a deeper knowledge of the structure of cellulose at nanoscale, as well as the potential combination of cellulose with other advanced materials, and therefore enabled many novel applications.[54] Through the appropriate processing of this biopolymer, many regenerated cellulose materials with different morphologies and properties can be produced, such as filaments, films, membranes, beads and hydrogels.[55] Due to the unique properties of cellulose, in particular biocompatibility and high versatility for chemical modification, it has also been used in diverse areas of biomedicine, showing great promise for drug

delivery applications.[7,44,56,57] In fact, cellulose has acknowledged potential for drug delivery due to its abundance of hydroxyl groups which can be easily functionalized in order to conjugate with drugs, imaging labels, and targeting ligands, such as folic acid, for example.[53,54] The latter can be of interest since cancer cells overexpress folate receptors in their plasma membrane which possess a high affinity for folic acid. Furthermore, this type of cellulose can be conjugated with considerable quantities of ionizable water-soluble drugs, such as tetracycline and doxorubicin.[57] The possibilities are endless, although thoroughly dependent on the choice of materials, drugs, surface modifications and the efficient reproduction of said assemblies.[23,32,33]

1.2.1. **Molecular structure**

Cellulose is a high molecular weight, water-insoluble, linear homopolymer that has been thoroughly studied since its discovery in 1838 by Anselme Payen.[33] Its molecular structure is responsible for various interesting properties, namely chirality, biodegradability, hydrophilicity and versatility for chemical modification conferred by the high reactivity of hydroxyl groups.[53,58] The polymeric chains of cellulose consist of repetitive core sequences of cellobiose, a dimer of two β-(1,4)-linked anhydro-D-glucose rings, with every unit being corkscrewed 180º relatively to its neighbors, as represented in Figure 7.[53]

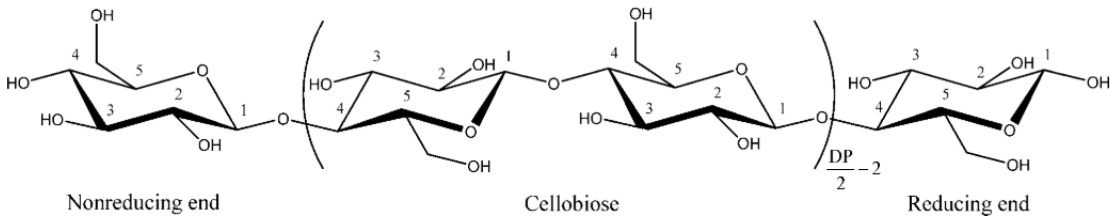

Figure 7*. Molecular structure of cellulose, showing the repetitive dimer, cellobiose, with carbon indexation, and the reducing and non-reducing ends. Image reprinted from reference [53].*

The β-D-glucopyranose rings possess a $^4C_1$ chair conformation, having the hydroxyl groups in the equatorial plane and the hydrogen atoms in the axial positions. These monomers are linked together through β(1→4) glycosidic bonds, which consists of an oxygen covalently bonded to the carbon atom C1 from one glucose monomer, and the carbon atom C4 of the adjacent unit.[54] The degree of polymerization (DP) reflects

the length of the chains by representing the number of polymerized glucose units $(C_6H_{10}O_5)_n$. The DP of cellulose can vary from 1000 to 30000 depending on the source and extraction method, reflecting chain lengths of 500 to 15000 nm, accordingly.[51] There are three reactive hydroxyl groups in every anhydro-D-glucose unit, one primary group at C6 and two secondary groups at C2 and C3, located in the ring plane. These are responsible for the establishment of intra- and intermolecular hydrogen bonds. In fact, the linear conformation of cellulose chains is supported by the intramolecular hydrogen bonding network between the neighboring glucose units, namely from the O(3′)-H hydroxyl group to the O(5) ring oxygen of the next monomer across the glycosidic linkage and also from the O(2)-H hydroxyl to the O(6′) hydroxyl of its neighbor.[53,54] This linearity favors the formation of parallel arrays of cellulose chains that are stabilized by intermolecular hydrogen bonds and consequently originate crystalline regions, or in other words, regions of highly ordered and periodic structural arrangements.[59]

1.2.2. **Crystallinity and hydrogen bonding patterns**

Within ordered regions, cellulose chains become tightly packed, forming crystallites. These are stabilized by Van der Waals interactions and strong hydrogen-bonding networks that can assume many different arrangements. For example, commercial cellulose (Avicel) can possess a crystallinity index varying from 39% to 67%, depending on the processing technique used.[60] Moreover, different cellulose polymorphs exist according to the respective treatments, sources, or methods of extraction.[53] A polymorph can be defined as a chemical substance which presents multiple distinct crystalline structures.[61] Crystalline materials present repetitive units, often called the unit cells of the crystal, and these vary among polymorphs, presenting various atomic spatial arrangements. To date, six interconvertible polymorphs of cellulose are known, namely, celluloses I, II, III_I, III_{II}, IV_I, and IV_{II}. These can be interconverted by the processes summarized in Figure 8.[62]

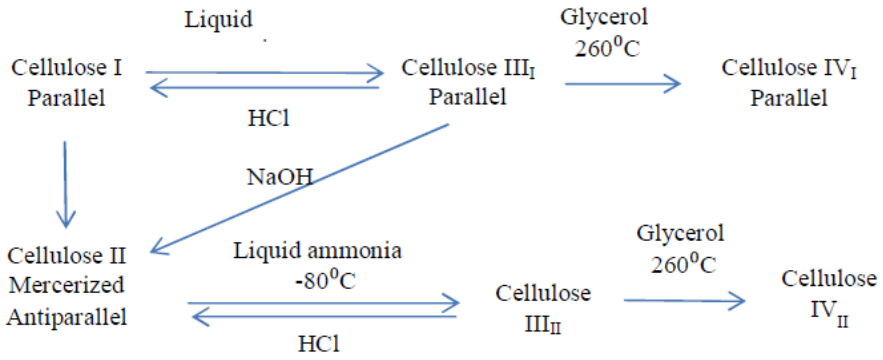

Figure 8*. Interconvertibility of cellulose allomorphs and their processing methods. Image reprinted from reference* [62].

Cellulose I, or native cellulose, occurs naturally, being produced by a plethora of different organisms, such as trees, plants, tunicates, algae, and bacteria. The model for the unit cell of cellulose I (native cellulose) was established by Kurt H. Meyer and Lore Misch in 1937 and was thereof known as the Misch-Meyer model, represented in Figure 9.[63]

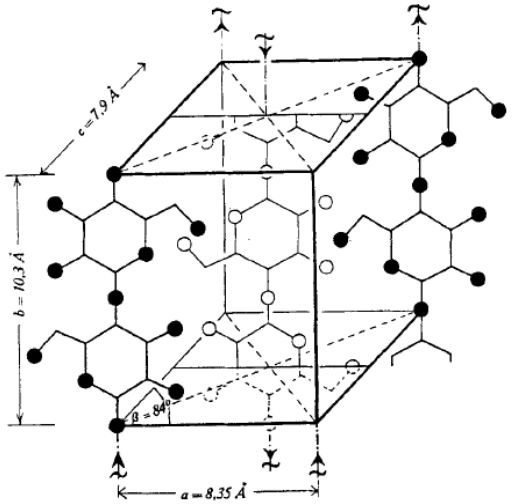

Figure 9. *Unit cell of cellulose I as described by the Misch-Meyer model. Image reprinted from reference* [63].

Cellulose II can be produced, from cellulose I, either by chemical regeneration (solubilization and recrystallization) or mercerization (aqueous sodium hydroxide treatments).[62] Cellulose II exhibits the highest stability among cellulose polymorphs, thus being technically more appealing for many applications.[54] Celluloses III$_I$ and III$_{II}$ can be obtained by treating either native or mercerized cellulose with liquid ammonia

which is posteriorly evaporated. As for celluloses IV_I and IV_{II}, these are obtained by heating celluloses III_I and III_{II} in glycerol at 260 °C, respectively.[64]

Further developments in computer and modeling technology enabled the refinement of the crystal structures of cellulose. Despite many publications regarding this matter, solid-state carbon cross polarization/magic angle spinning (^{13}C CP/MAS) nuclear magnetic resonance (NMR) data presented some contradictory results among researchers. To explain those differences, it was deducted that native cellulose was comprised of a system of two distinct crystalline phases: Iα and Iβ. These two sub-allomorphs can co-exist in the same cellulose sample or even the same microfibril with different ratios depending on their source. Cellulose Iα presents a triclinic unit cell with one chain, while cellulose Iβ possesses a monoclinic unit cell containing two parallel chains. Both allomorphs present parallel configurations but different hydrogen bonding patterns, therefore leading to different crystalline arrangements, as presented in Figure 10.[65,66]

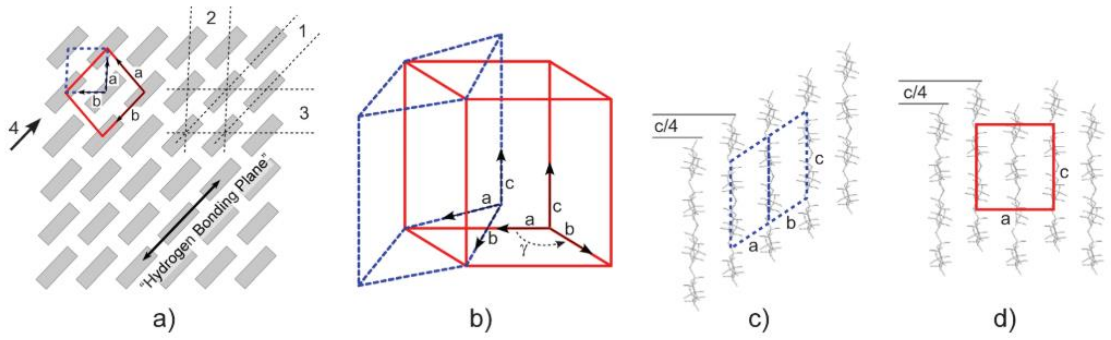

***Figure 10**. Unit cells of cellulose Iα (triclinic, dashed blue line) and Iβ (monoclinic, solid red line): a) projected in the cellulose I crystal lattice with planes 1, 2, and 3 representing the three major lattice planes, with d-spacings of 0.39, 0.53, and 0.61, respectively; b) Relative spatial confirmation of Iα in comparison to Iβ; c) Hydrogen-bonding sheet displacement for Iα; and d) for Iβ. Image reprinted from reference [54]*

The determination of hydrogen bonding networks is not an easy task, and findings also present some discordance between researchers, although a consensus is slowly being achieved. To date, Nishiyama and colleagues presented the most accurate structural determinations of the crystal lattices of Iα and Iβ using synchrotron X-ray and neutron fiber diffraction.[65–67] Cellulose Iα occupies the lattice planes $(110)_t$, $(010)_t$, and $(100)_t$ while Iβ occupies $(200)_m$, $(110)_m$, and $(110)_m$. As the hydroxyl groups of cellulose are located equatorially with respect to the ring plane the intra- and inter-chain

hydrogen bonding mostly occurs in the $(110)_t$ and $(200)_m$ planes, thus being called the "hydrogen-bonded plane" mentioned in Figure 9a). The proposed hydrogen bonding networks for these structures in said plane are displayed in Figure 11.

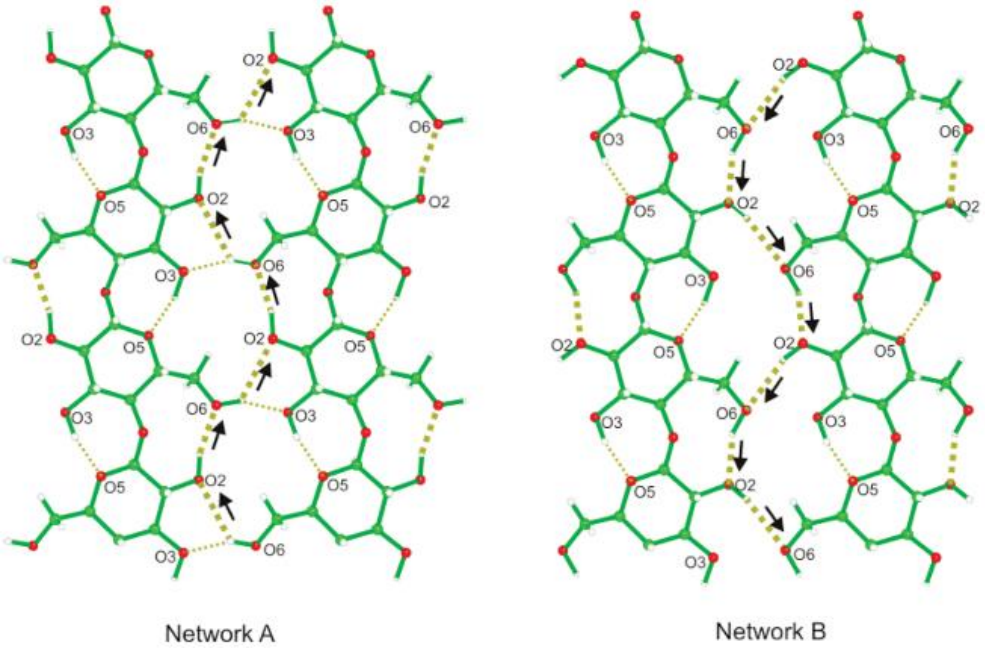

Figure 11. *Representation of the suggested cooperative hydrogen bonding networks A, and B, in the "hydrogen-bonded plane". Thick dotted lined represent inter-chain bonds while thin dotted lines represent the intra-chain bonds. Image reprinted from reference* [67].

1.2.3. **Supramolecular structure**

Cellulose presents a hierarchical structure responsible for its remarkable mechanical properties. The structure-property-function relationship of this architecture is of tremendous importance in order to understand the possible applications and handling of this polymer.[68] In this matter, cellulose fiber and microfibrils possess alternating crystalline and amorphous regions, held together through hydrogen bonds and van der Waals forces.[54,68] Generally, 36 cellulose chains are assembled into elementary fibrils, commonly known as protofibrils (~10 nm in diameter). These protofibrils are brought together into microfibrils (ranging from 5-50 nm in diameter), which in turn are aggregated into macrofibers (~10 µm in diameter) that compose the cell walls of wood, along with hemicellulose and lignin.[53,54,69] This hierarchy is illustrated in Figure 12.

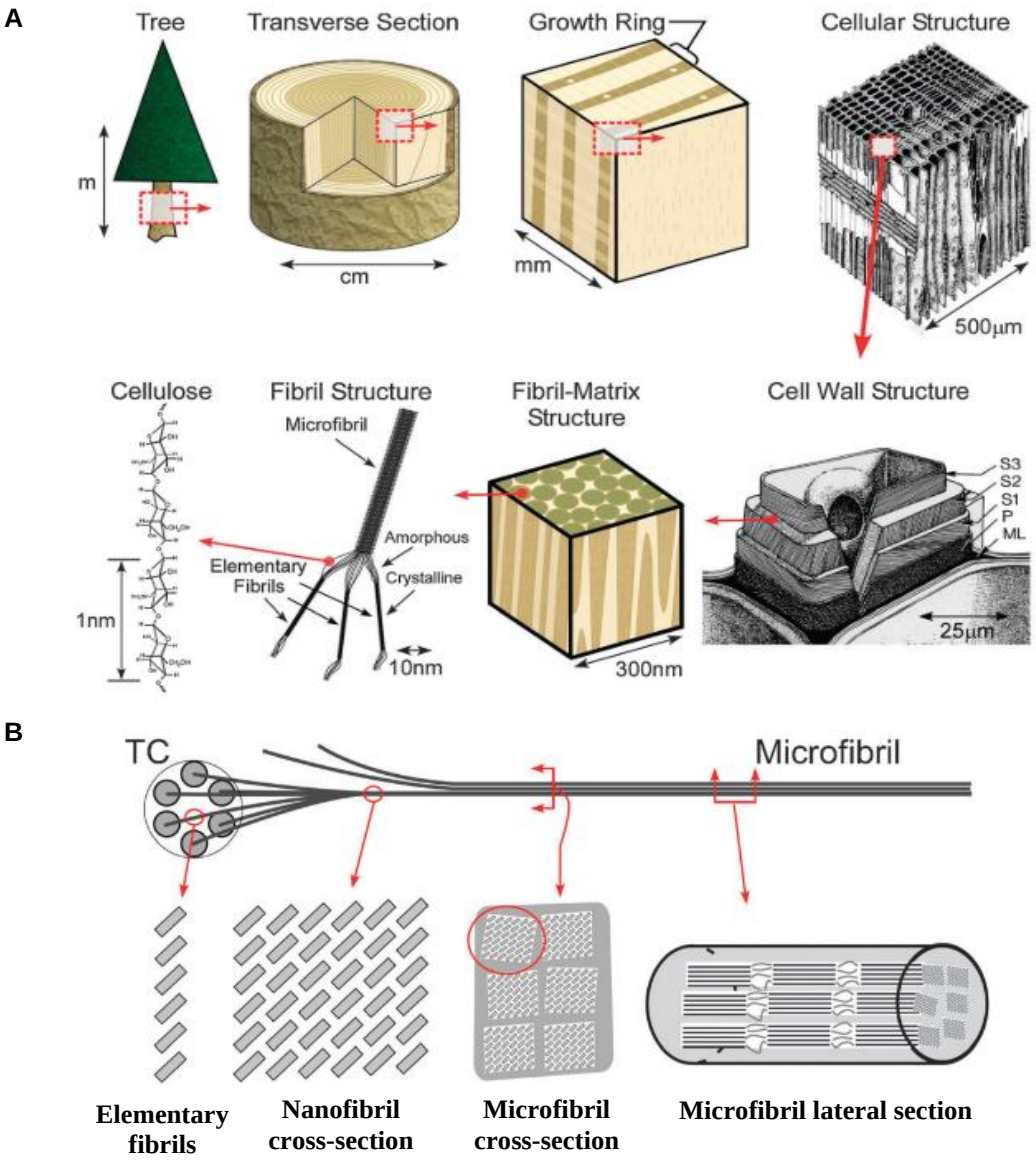

Figure 12. *A) Hierarchical structure of wood cellulose; B) Microfibrillar structure of cellulose. Each grey rectangle represents the cross-section of a cellulose chain. Image adapted from reference* [54].

1.2.4. **Cellulose-based materials**

Through proper processing, cellulose can be transformed into a plethora of different materials with varying properties for different ends.[70,71] Essentially, the dissolution, and shaping of cellulose or its derivatives through regeneration, results in distinct shapes such as fibers, films, beads, aerogels, and hydrogels.[55] Cellulose fibers, for example, have been widely used in everyday life for a long time, namely as textiles fabrics.[55] Hydrogels and aerogels are produced by physical aggregation followed by

chemical cross-linking, producing hydrophilic, biocompatible, and cheap platforms often used in tissue engineering.[72,73] Finally, cellulose spheres or beads are typically produced by dissolution and regeneration, and can be used in chromatography[74], biocatalyst immobilizations[75], among other applications.[55] However, the inherent intra- and interchain hydrogen bonds of cellulose, in addition to the intersheet Van-der-Waals interactions make cellulose insoluble in water and other common solvents. In order to convert cellulose into added-value products, dissolution is often carried out, in which traditional aqueous and nonaqueous solvents, such as sodium hydroxide/carbon disulfide mixtures, *N*-methylmorpholine oxide (NMMO), dimethyl sulfoxide (DMSO)/tetrabutylammonium fluoride (TBAF), and aqueous solutions of metal complexes, are employed.[76] However, they present disadvantages, such as high cost, toxicity, volatility, poisonous gas generation, non-recyclability, and lack of insufficient solvation potential.[77] For these reasons, industrial chemical processes are hallmarked by the need for sustainability and eco-efficiency, employing green chemistry whenever possible.[78,79]

With respect to its application in cancer therapy, there are two nanoscale forms of cellulose that stand out, namely cellulose nanocrystals (CNCs) and cellulose nanofibers (CNFs). Transmission electron micrographs of both nanometric forms are shown in Figure 13.[80] CNCs consist of NPs with the shape of rods or whiskers mostly produced by acid hydrolysis of wood and plant fiber. On the other hand, CNFs are nanosized cellulose fibrils that are obtained when certain techniques are applied to the mechanical refining of wood and plant cellulose.[54]

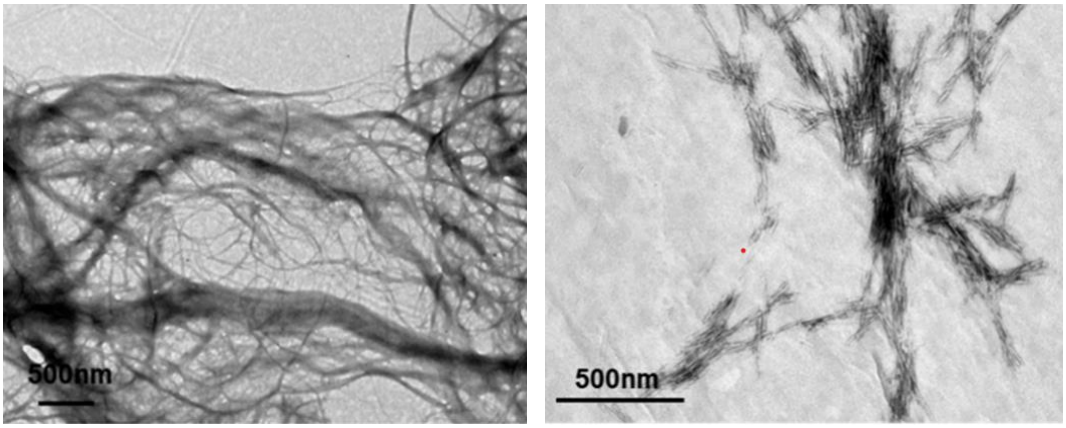

Figure 13*. Transmission electron micrographs of cellulose nanofibers (left) and cellulose nanocrystals (right). Adapted from reference* [80].

In this regard, Hu *et al*.[81] developed rod-like CNCs with redox-responsive polycations for gene delivery applications, exhibiting good activity for suppression of cancer cell growth. In a different work, Svagan *et al*. and Löbmann *et al*. prepared CNF films by casting a drug/CNF suspension and performing a subsequent drying step. The produced films showed an immediate drug release of the poorly water-soluble model drug indomethacin, for drug delivery applications.[82,83]

Other cellulose-based material with special interest for the present work is cellulose beads. These are spherical particles with varying sizes that can range from the nanoscale up to several millimeters, which are commonly prepared through dissolution, and regeneration (shaping) of cellulose when using its derivatives. Generally, the shaping of cellulose or its derivatives into beads can be summarized into three pathways, as shown in Figure 14.[84]

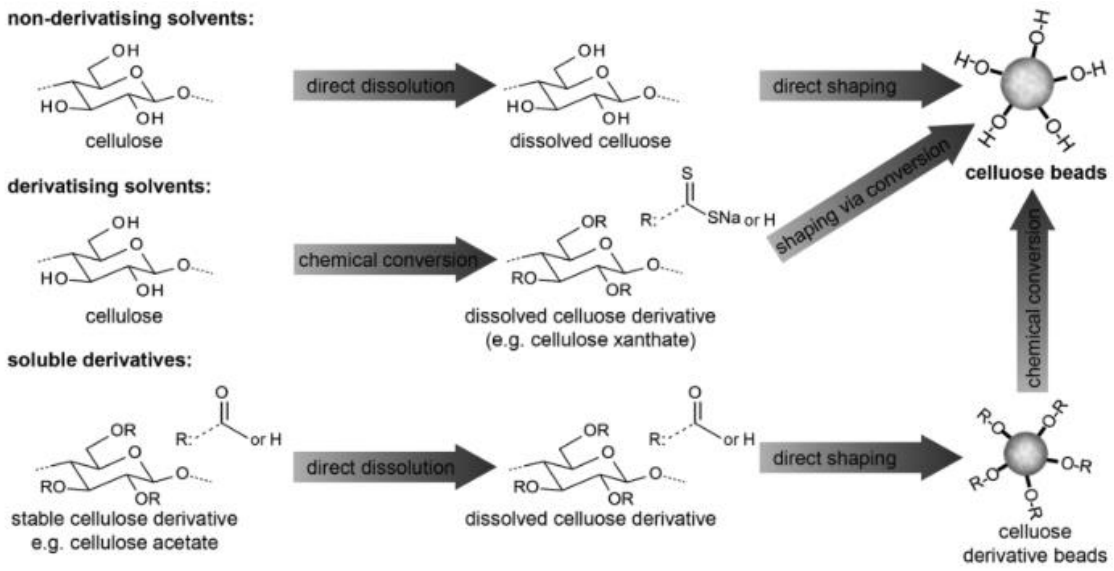

Figure 14*. Pathways for cellulose dissolution and reshaping into beads. Image reprinted from reference* [84].

Non-derivatizing solvents achieve cellulose dissolution through physical interactions, therefore, leaving its hydroxyl groups chemically untouched. In this case, polymer regeneration is achieved by disturbing these interactions, for example, by coagulation in an excess of protic nonsolvent.[84,85] As for derivatizing solvents, these temporarily transform cellulose into derivatives that are usually only metastable. Consequently, it is possible to shape cellulose into objects, like fibers or beads, by cleaving of the intermediate derivatives, through the addition of water or a change in pH

or temperature.[84,86] Finally, it is feasible to prepare shaped cellulosic systems through the use of stable cellulose derivatives, such as cellulose acetate, that are soluble in common organic solvents and generally commercially available. Following the shaping of the solution into particles, the cellulose derivative is regenerated through coagulation or solvent evaporation in the presence of a nonsolvent.[84] In this case, an additional step is needed to convert the shaped derivative into the corresponding cellulose beads, for example by alkaline hydrolysis.[84,87]

Table 1 summarizes several cellulose-based beads systems for distinct applications, giving insight on the type of cellulose, preparation methods, use of additives, as well as the shapes and sizes of the materials.

Table 1. *Overview of cellulose beads systems for varying applications.*

Material	Preparation method	Additives	Shape and Sizes	Application	Refs
Cellulose	Sol-gel	Ag-Fe_3O_4 nanoparticles	Spherical 10-20 µm	Catalysis	88
	Coagulation	γ-Fe_2O_3 nanoparticles	Spherical 2.89 mm	Food industry	89
	Coagulation	Ranitidine hydrochloride	n.a.	Drug delivery	90
	Coagulation	Curcumin	Spherical 0.81 -4.60 mm	Drug delivery	91
	Emulsification	Gold nanoparticles (AuNPs); Antibody conjugation.	Spherical 160-170 nm	Cancer theranostics	37
	Precipitation	Cellulose nanocrystals (CNCs)	Spherical 0.67 – 1.62 mm	Wastewater treatment; Chromatography; Food and drug industries.	92
Cellulose acetate	Microfluidics/ Flash-freezing	n.a.	Spherical 270 µm	Pollutant adsorption	93
Bacterial cellulose	Culture of *K. xylinus*	Poly(ethyleneimine); Ferromagnetic particles	n.a.	Enzyme immobilization	75
	Microfluidics	n.a.	Spherical 50 µm	Wound healing	94
Carboxymethyl cellulose	Inverse suspension	Epichlorohydrin	Spherical 72–84 µm	Wastewater treatment	95

For example, the work of Metaxa *et al*.[96] created hollow beads based on a cellulose derivative, hydroxypropyl cellulose, that were functionalized with folic acid with the intent of binding to overexpressed receptors of cancer cells for drug delivery. Micrographs of the produced hollow spheres are shown in Figure 15. The produced particles exhibited an efficient drug encapsulation and multi-stimuli drug releasing capabilities, thus, evidencing a promising drug delivery agent.[96]

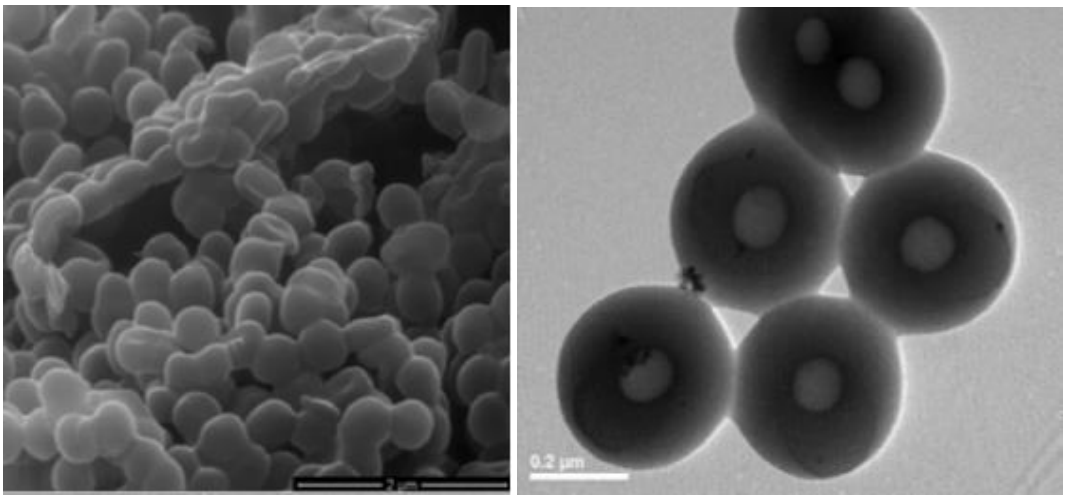

Figure 15. *Hydroxypropyl cellulose-based hollow beads for drug delivery applications. Adapted from* [96].

In another study, Carrick *et al*.[37] prepared cellulose nanobeads with encapsulated gold nanoparticles (AuNPs) for theranostic purposes. In addition, the surface of the produced nanospheres was conjugated with an antibody possessing specificity to the epidermal growth factor receptor protein to promote interaction with cancer cells. AuNPs act as a contrast agent, for cell imaging applications, thus, rendering the developed system a potential theranostics device. The general working principle of these nanospheres is represented in Figure 16.

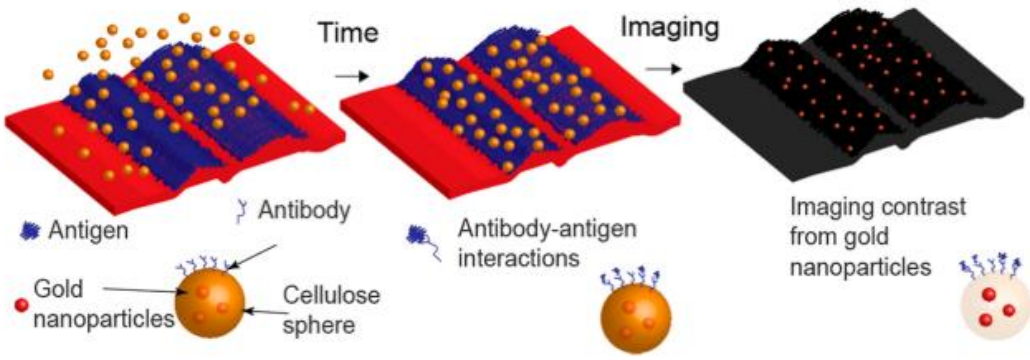

***Figure 16**. Schematic representation of the working principle of the immunoselective cellulose nanospheres for theranostic application. Image reprinted from reference [37].*

1.3. Motivation and objectives

In this context, cellulose nanobeads stand out as promising biocompatible, biodegradable, and chemically versatile nanomaterials for several biomedical applications. Inspired by this idea, the present dissertation aims to develop multifunctional cellulose-based nanobeads for potential application in cancer diagnostic and treatment. These cellulose nanobeads will present a spherical shape, and their surface will be functionalized with gold nanoparticles that will play the dual role of cell imaging and therapeutic agent (Figure 17).

Given the high chemical resistance and insolubility of cellulose in most common solvents that hamper the production of micro/nanoparticles with specific shape and size,[97] the cellulose nanobeads will be prepared through the use of cellulose acetate (CA) as the starting raw-material instead of directly using cellulose. So, CA nanobeads will be obtained by nanoprecipitation,[98] involving CA dissolution, regeneration and hydrolysis, as illustrated in Figure 14.

Then, the cellulose nanobeads/AuNPs hybrid systems will be prepared via two methodologies, namely by regenerating the CA in the presence of the AuNPs followed by alkaline hydrolysis, and by performing an *in situ* synthesis of the AuNPs in the presence of the hydrolyzed CA (Figure 17). Moreover, these nanohybrid systems will be characterized in terms of morphology, size, and *in vitro* cytotoxicity, to assess their potential for the intended application.

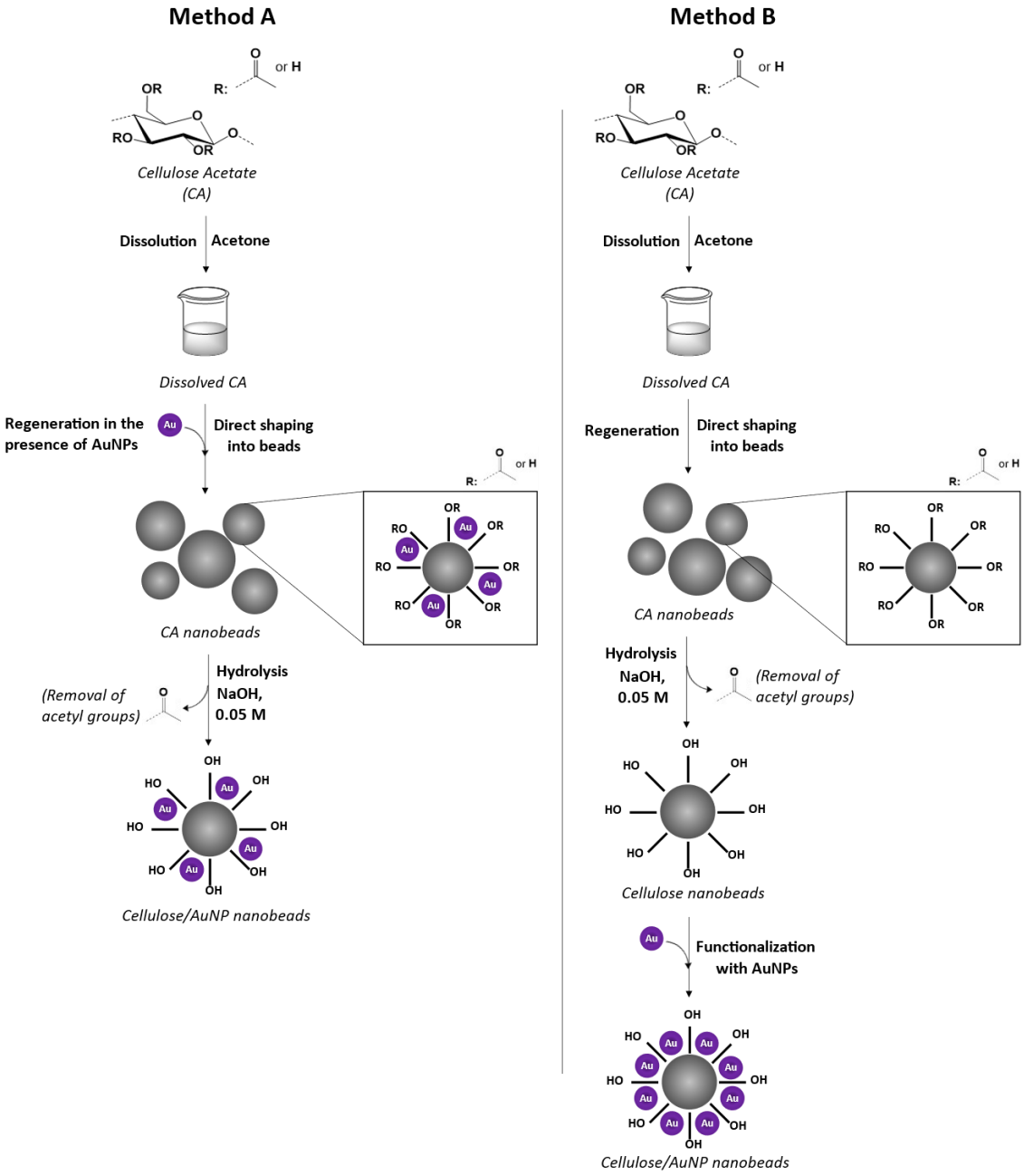

Figure 17*. Schematic representation of the two methodologies carried out to achieve the production of cellulose nanobeads/AuNPs hybrids for imaging and therapeutic applications.*

CHAPTER 2 – EXPERIMENTAL PART

The present chapter will consist of a thorough description of the materials and experimental procedures followed throughout the study. The techniques used to characterize both the starting materials and all the materials prepared in this study, namely the cellulose acetate, the cellulose nanobeads, the AuNPs and the cellulose nanobeads/AuNPs hybrids, are also described here.

2.1. Chemicals and materials

Cellulose acetate (CA) membranes (diacetate substituted type, soluble in acetone) were purchased from FILTER-LAB®. Tri-sodium citrate dihydrate ($Na_3C_6H_5O_7 \cdot 2H_2O$, 99%) was purchased from BDH®. Chloroauric acid ($HAuCl_4$, ≥99.9%), acetone (CH_3COCH_3, ≥99.5%), dimethyl sulfoxide (DMSO), and 3-(4,5-dimethylthiazol-2-yl)-2,5-diphenyltetrazolium bromide (MTT, 98%) were obtained from Sigma-Aldrich. Sodium hydroxide (NaOH, 98.5%) was purchased form ACROS Organics™. Phosphate buffer saline (PBS, pH 7.4), Dulbecco′s Modified Eagle′s Medium (DMEM), fetal bovine serum (FBS), L-glutamine, penicillin, streptomycin, and amphotericin B were supplied by Gibco® (Life Technologies, Grand Island, NY, USA). Type 1 ultrapure water (resistivity of 18.2 MΩ cm (25 °C)) was filtered using a Simplicity® Water Purification System (Merck Millipore, Darmstadt, Germany).

The pigmented human melanoma (MNT-1) cell line was kindly provided by Doctor Manuela Gaspar from the Research Institute for Medicines (iMed.ULisboa), Faculty of Pharmacy, University of Lisbon, Portugal.

2.2. Production of cellulose nanobeads: dissolution, regeneration, and hydrolysis of cellulose acetate

The production of the cellulose nanobeads is divided into three stages, namely the dissolution, regeneration, and hydrolysis of CA, as exemplified in Figure 18. Briefly, CA (79 mg) was dissolved in 20 mL of acetone under magnetic stirring at 500 rpm. Then, the regeneration of CA was performed following the water-on-polymer

method, as described by Wondraczek *et al*.[98] Using a syringe with a 0.45 mm needle gauge, distilled water (15 mL) was added dropwise to the CA solution (5 mL, 3.95 mg mL^{-1}) under continuous stirring at 500 rpm. Then, the resulting mixture was heated in an oil bath at 70 °C for 2 h to fully evaporate acetone. After this step, approximately 15 mL of a CA beads suspension is obtained, with an approximate CA concentration of 1.33 mg mL^{-1}.

In order to remove the acetate groups of CA and convert it into cellulose, an alkaline hydrolysis was carried out.[99] The regenerated CA nanobeads suspension (4 mL, 1.33 mg mL^{-1}) was hydrolyzed using a NaOH solution (4 mL, 0.05 M) under magnetic stirring at 500 rpm for 15 min. As soon as the reaction time was due, 16 mL of distilled water were added to the mixture to stop the hydrolysis reaction. Afterwards, the nanobeads were centrifuged at 6000 rpm for 15 min and the supernatant was carefully removed. The nanobeads were then resuspended in distilled water and centrifuged again. This process was repeated 3 to 4 times to ensure the removal of the NaOH residues.

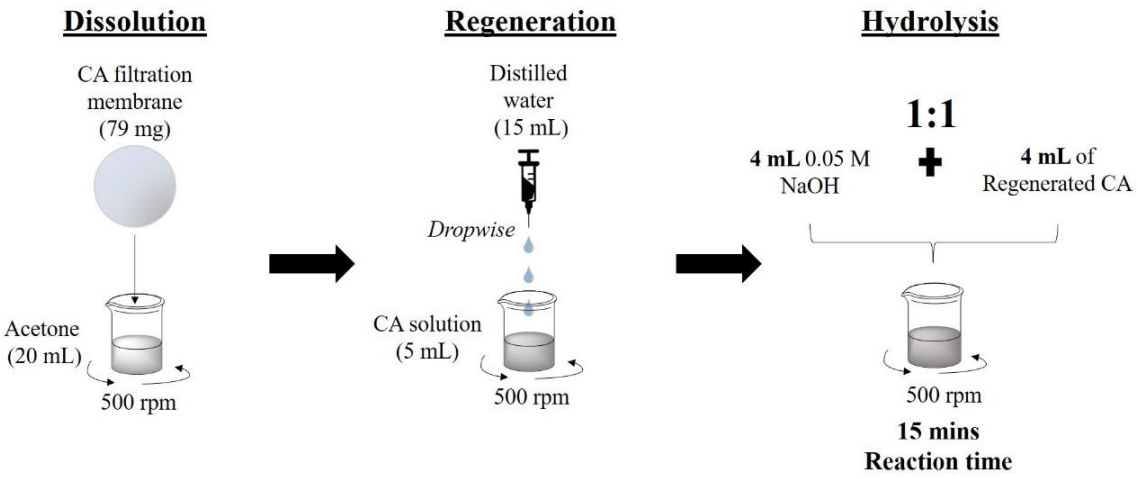

***Figure 18**. Schematic representation of the dissolution, regeneration, and hydrolysis of CA to produce cellulose nanobeads.*

2.3. Synthesis of gold nanoparticles (AuNPs)

The AuNPs were obtained by reduction of a gold(III) complex using sodium citrate.[100] An aqueous solution of sodium citrate (188 µL, 0.085 M) was added dropwise to a chloroauric acid aqueous solution (10 mL, 0.24 mM) at 80 °C, under magnetic

stirring at 500 rpm and left overnight. On the following day, the mixture displayed a bright red color. To remove the residues of sodium citrate present in the mixture, the particles were centrifuged at 15000 rpm for 30 mins at 4 °C, and the supernatant was carefully removed using a micropipette. The particles were then resuspended in Milli-Q water and centrifuged again. This process was repeated 3 times to ensure the removal of all remaining sodium citrate.

2.4. Preparation of the cellulose nanobeads/AuNPs hybrids

The cellulose nanobeads/AuNPs hybrids were prepared via two methodologies, namely the regeneration of CA in the presence of AuNPs followed by alkaline hydrolysis, and the *in situ* synthesis of the AuNPs in the presence of the cellulose nanobeads.

2.4.1. Method A: Regeneration of CA in the presence of AuNPs followed by alkaline hydrolysis

The AuNPs previously synthetized in section 2.3 were resuspended in acetone and added to the CA solution considering a mass ratio 1:8 between Au and cellulose nanobeads. The regeneration procedure was then carried out as described in section 2.2, followed by acetone evaporation. Subsequently, the resulting mixture is hydrolyzed according to the procedure described in section 2.2 to remove the acetyl groups of CA.

2.4.2. Method B: *In situ* synthesis of the AuNPs in the presence of the cellulose nanobeads

In this methodology, the AuNPs were synthesized in the presence of the cellulose nanobeads that were prepared in section 2.2. The same mass ratio of 1:8 of AuNPs/cellulose nanobeads was selected and the synthesis followed all the steps described in section 2.3.

2.5. Characterization techniques

The materials produced along this work, namely CA nanobeads, hydrolyzed CA nanobeads, AuNPs, and cellulose nanobeads/AuNP hybrids were characterized using several techniques, namely attenuated total reflection-Fourier transform infrared (ATR-FTIR) spectroscopy, scanning electron microscopy (SEM), scanning transmission electron microscopy (STEM) and ultraviolet-visible (UV-Vis) spectroscopy.

2.5.1. Attenuated total reflection-Fourier transform infrared (ATR-FTIR) spectroscopy

ATR-FTIR spectra were recorded with a Perkin-Elmer FT-IR System Spectrum BX spectrophotometer (Perkin-Elmer Inc., Massachusetts, USA) equipped with a single horizontal Golden Gate ATR cell, over the range of 600–4000 cm^{-1} at a resolution of 4 cm^{-1} over 32 scans.

2.5.2. Scanning electron microscopy (SEM) and scanning transmission electron microscopy (STEM) coupled with energy dispersive X-ray spectroscopy (EDS)

SEM and STEM micrographs were obtained with a HR-SEM-SE SU-70 Hitachi microscope (Hitachi High-Technologies Corporation, Tokyo, Japan) operating at 4 kV for the cellulose materials and at 15 kV for the gold nanoparticles. The microscope is equipped with a microanalysis Bruker QUANTAX 400 detector (Bruker Nano GmbH, Berlin, Germany) for EDS. The samples were placed on a steel plate and coated with a carbon film prior to SEM analysis, and on a carbon-coated copper grid for STEM analysis. The size of the samples was determined from the SEM micrographs through ImageJ Software analysis.

2.5.3. Ultraviolet-visible (UV-Vis) spectroscopy

Optical spectra were recorded by a Thermo Scientific Evolution 220 spectrophotometer (Thermo Fisher Scientific, Waltham, MA, USA) using 100 scans min^{-1} with a bandwidth of 2 nm and an integration time of 0.3 s.

2.6. In vitro cytotoxicity assays

The *in vitro* cytotoxicity of the cellulose nanobeads and cellulose nanobeads/AuNPs hybrid obtained by the *in situ* synthesis of AuNPs in the presence of the cellulose nanobeads was assessed by the colorimetric MTT assay, which measures the formation of purple formazan in viable cells.[101]. The pigmented human melanoma (MNT-1) cell line was cultured in DMEM supplemented with 10% fetal bovine serum, 2 mM L-glutamine, 100 U mL^{-1} penicillin, 100 µg mL^{-1} streptomycin, and 2.5 µg mL^{-1} amphotericin B. Cells were incubated in a humidified atmosphere of 5% CO_2 at 37 °C. Sub confluent cells were trypsinized with trypsin-EDTA (0.25% trypsin, 1 mM EDTA) when monolayers reached 70% confluence.

Cells were seeded in 96-well plates and after 24 h, medium was replaced with fresh medium containing cellulose nanobeads (4.9, 9.8, 19.5 and 39.0 µg mL^{-1}) or cellulose nanobeads/AuNPs hybrid (4.9, 9.8, 19.5 and 39.0 µg mL^{-1}), and cell viability was measured after 24 h. After that, 50 µL of MTT reagent (1 mg mL^{-1}) in PBS was added to each well and incubated for 4 h at 37 ℃, and 5% CO_2. The medium was then removed, and 150 µL of DMSO was added to each well for crystal solubilization. The optical density of the reduced MTT was measured at 570 nm in a microtiter plate reader (Synergy HT Multi-Mode, BioTeK, Winooski, VT), and the cell metabolic activity (a usual marker for cell viability) was calculated as:

$$Cell\ metabolic\ activity\ (\%) = \frac{(Abs_{sample} - Abs_{DMSO})}{(Abs_{control} - Abs_{DMSO})} \times 100.$$

Three independent assays were performed with at least 3 technical replicates each and the results compared with the control (incubated with culture medium).

CHAPTER 3 – RESULTS AND DISCUSSION

The present study intended to develop multifunctional spherical cellulose-based nanobeads for potential application in cancer diagnosis and treatment. Spherical cellulose nanobeads were functionalized with gold nanoparticles (AuNPs) that will act simultaneously as imaging and therapeutic agent. The application of AuNPs as cell imaging agent has received considerable interest, being able to be detected by multiple techniques, such as dark field microscopy, light microscopy, fluorescent imaging, surface-enhanced Raman spectroscopy, and enhanced X-ray scatter imaging.[37] The potential of AuNPs as therapeutic agent can employ thermotherapy via near infrared light absorption and consequent heat generation, that will promote the killing of the tumor cells.[102] The hereby obtained cellulose nanobeads/AuNPs hybrid systems were characterized in terms of morphology, size and *in vitro* cytotoxicity towards the pigmented human melanoma (MNT-1) cell line.

3.1. Preparation and characterization of the cellulose nanobeads

The cellulose nanobeads were prepared through the use of cellulose acetate (CA) as the starting raw-material instead of directly using cellulose, because of the high chemical insolubility of cellulose in most common solvents that hamper the production of micro/nanoparticles with specific shape and size.[97] CA is a commercial cellulose ester obtained by acetylation of cellulose and can be synthesized with different degrees of substitution, namely mono-, di- or tri-acetate, which translates into polymers that are soluble in different solvents.[103] While cellulose triacetate and diacetate are soluble in organic solvents like dichloromethane and acetone, respectively, the cellulose mono-acetate is water soluble. Furthermore, this cellulose ester is considered a non-toxic, and biodegradable polymer and, thus, is being applied in the biomedical field.[103] As a result, the diacetate substituted type of CA was selected because of the previously enumerated properties, alongside its solubility in acetone that is a less harmful organic solvent.

The CA nanobeads were obtained by nanoprecipitation, as described by Wondraczek and coworkers,[98] and the methodology can be divided into three stages, namely CA dissolution, regeneration and hydrolysis, as illustrated in Figure 19. The

dissolution of CA was performed in acetone and was followed by regeneration via the water-on-polymer method,[98] where an excess of water was added dropwise with a syringe to the CA acetone solution. Then, the resultant CA nanobeads were submitted to an alkaline hydrolysis to yield cellulose nanobeads (Figure 19). Herein, two hydrolysis times (15 and 30 min) were investigated, and the optimized parameter (15 min) was chosen by reaching a compromise between the extent of the hydrolysis reaction and the obtainment of spherical nanobeads without the formation of agglomerates.

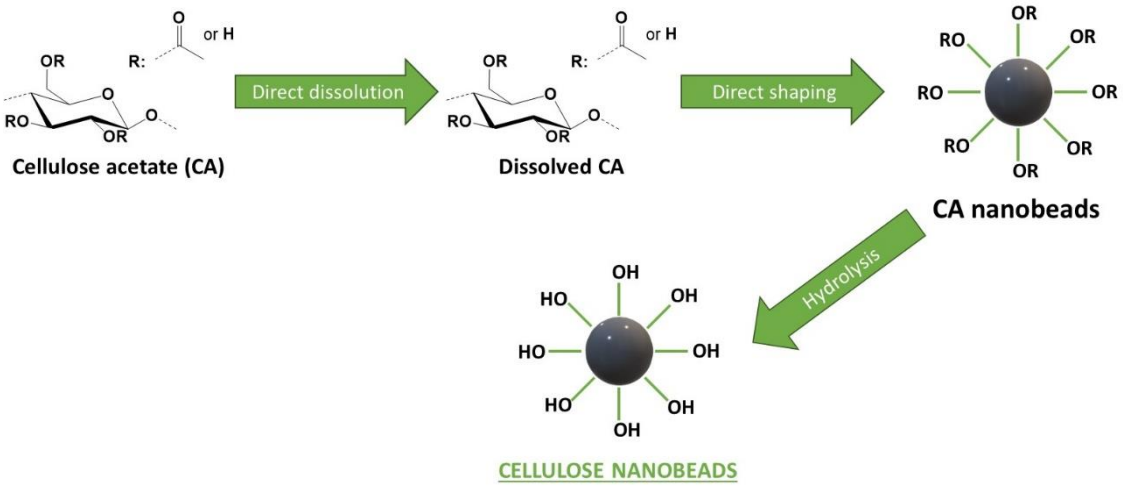

***Figure 19**. General route for cellulose acetate dissolution, regeneration (shaping into nanobeads) and hydrolysis, yielding cellulose nanobeads.*

The produced cellulose nanobeads were then characterized regarding their structure by attenuated total reflection-Fourier transform infrared (ATR-FTIR) spectroscopy, and morphology by scanning electron microscopy (SEM), as discussed in the following paragraphs.

The structural characterization of the cellulose acetate, regenerated CA, and hydrolyzed CA was carried out by ATR-FTIR vibrational spectroscopy that gives information about their functional groups. As anticipated, and according to Figure 20, the ATR-FTIR spectra of CA and regenerated CA are totally equivalent, revealing the presence of three distinct absorption bands at 1740, 1370, and 1220 cm^{-1}, which are assigned to the C=O stretching of the acetyl group, C–H bending of the CH_3 in the acetyl group, and the C–O stretching of the acetyl group, respectively.[104] Therefore, the dissolution and regeneration processes have no effect on the chemical structure of CA.

This was expected as the dissolution and regeneration processes employed in this study do not change the chemical structure or the functional groups of CA.

Then, the alkaline hydrolysis of the regenerated CA nanobeads was also validated by ATR-FTIR spectroscopy. Based on Figure 20, the CA hydrolysis led to an increase in the band intensity of the hydroxyl groups in the region of 3600-3200 cm^{-1}. Moreover, there is a significant decrease of the intensity regarding the absorption bands at around 1740 and 1220 cm^{-1}, which are allocated to the C=O and C–O stretching vibrations of the acetyl group, respectively. Hence, it is possible to conclude that the presented methodology successfully converted some of the acetyl groups at the surface of the regenerated CA nanobeads into hydroxyl groups. These results are in accordance with other works involving the alkaline hydrolysis of CA-based materials.[87,99]

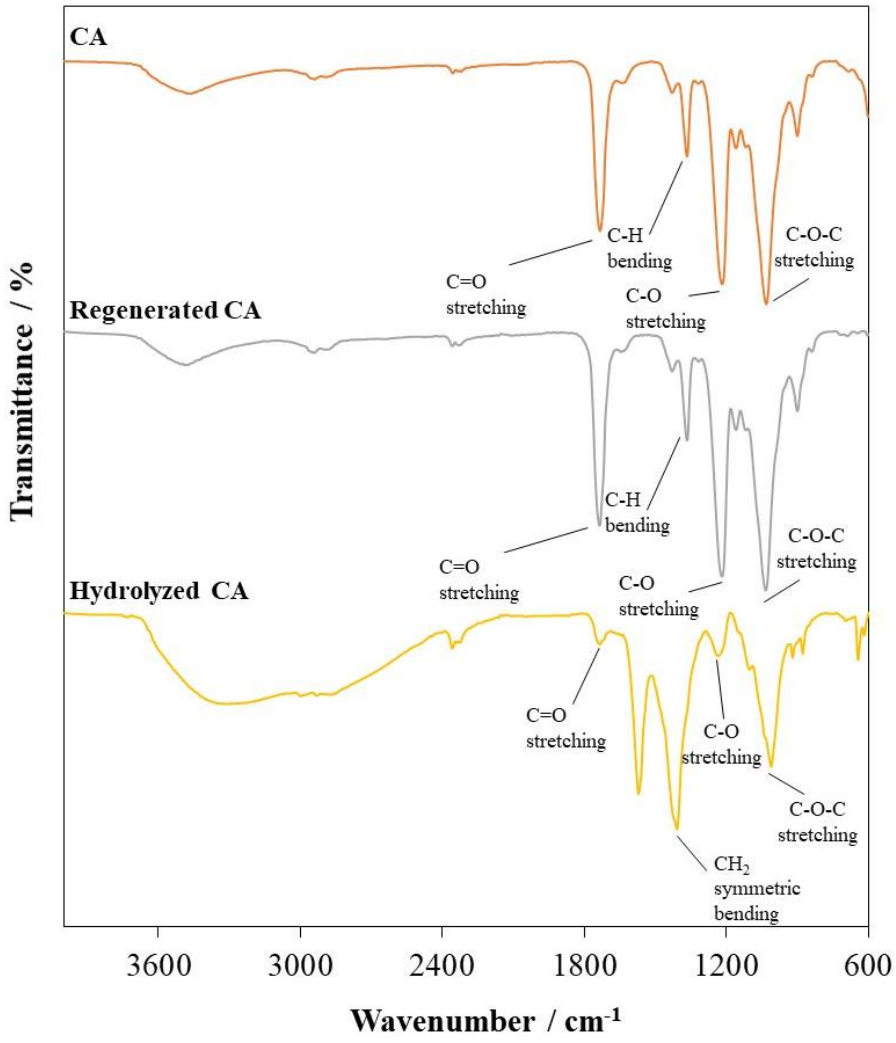

***Figure 20**. ATR-FTIR spectra of cellulose acetate, regenerated CA, and hydrolyzed CA.*

The morphology and size of the nanobeads were evaluated by SEM, as depicted in Figure 21 and Figure 22 for the regenerated and hydrolyzed CA nanobeads, respectively. The regenerated CA beads show a well-defined spherical shape with a smooth surface (Figure 21). Although the size distribution is not narrow, the beads exhibit an average size of 456±185 nm, which is in tune with the data reported by Wondraczek and coworkers.[98]

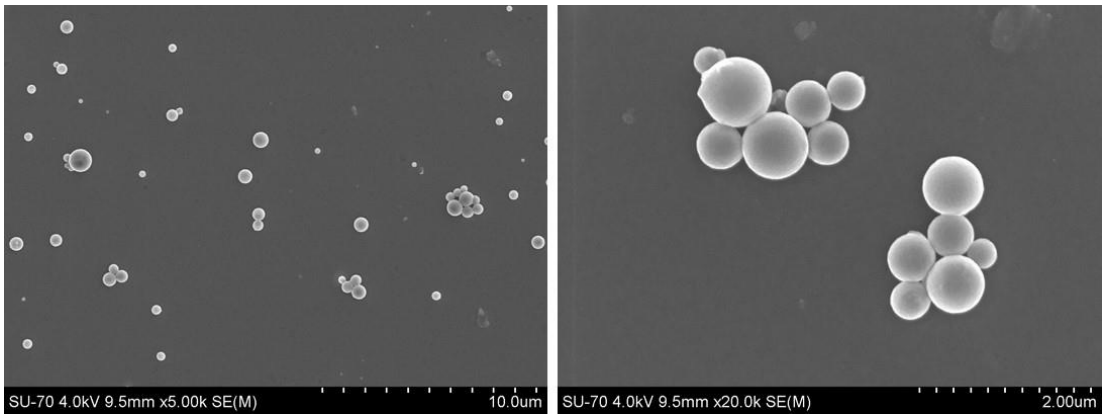

Figure 21. *SEM micrographs of the regenerated CA nanobeads.*

Regarding the hydrolyzed CA nanobeads, *i.e*. the cellulose nanobeads (Figure 22), they preserved the well-defined spherical shape and broad size distribution, yielding an average size of 440±190 nm showing that the mild alkaline hydrolysis did not affect the morphology and size of the cellulose nanobeads.

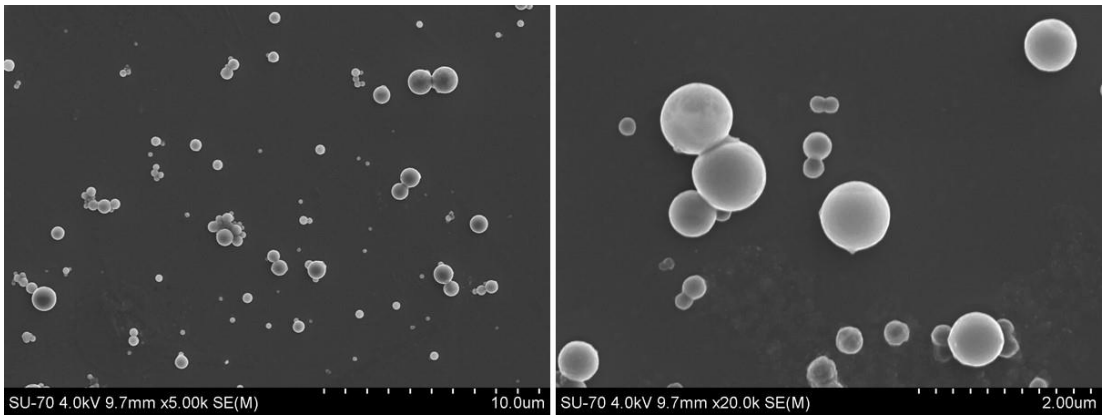

Figure 22. *SEM micrographs of the hydrolyzed CA nanobeads, i.e. the cellulose nanobeads.*

3.2. Synthesis and characterization of the gold nanoparticles

Following the investigation of the feasibility of developing cellulose nanobeads, the subsequent stage is focused on studying the synthesis of gold nanoparticles (AuNPs), and their characterization in terms of optical properties by ultraviolet-visible spectroscopy (UV-vis), and morphology and size by SEM in transmission mode (STEM). The AuNPs were chosen because of their biocompatibility, non-immunogenicity, easy synthesis, and the simultaneous potential for cell imaging and cancer treatment, as previously mentioned.[105]

The colloidal AuNPs were synthesized using sodium citrate as reducing and capping agent.[100] The color change of the Au solution from pale yellow to ruby red is a first confirmation of the successful formation of the AuNPs, as illustrated in the inset photograph of the colloidal solution of AuNPs in Figure 23. In fact, it is largely reported in literature that the colloidal AuNPs exhibit different colors depending on their size, shape, and aggregation state, as reviewed by Huang and El-Sayed.[106]

The AuNPs were then analyzed by UV-Vis spectroscopy and the spectrum (Figure 23) presents a band centered at 520 nm, which is attributed to the surface plasmon resonance (SPR) of gold nanoparticles.[100] The SPR originates from the collective oscillation of the electrons of the conduction-band after resonant excitation by incident photons,[105] and confirms the successful synthesis of the AuNPs.

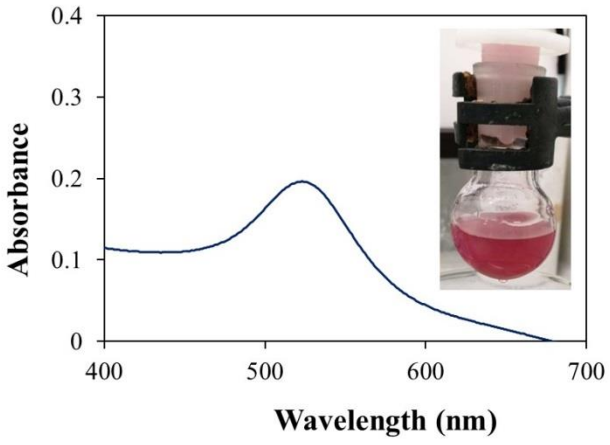

Figure 23*. UV-Vis absorption spectrum of the AuNPs, and digital photograph of the colloidal dispersion of AuNPs.*

Additionally, the morphology and size of the AuNPs were analyzed by STEM, as depicted in Figure 24. The synthetized AuNPs revealed individualized and spherical

shaped nanoparticles with an average size of 13.0±1.7 nm, which is in agreement with the values found by Pinto and coworkers.[100] Furthermore, and considering the data reported in literature, this average size value was clearly expected because, as examined by Link and El-Sayed,[107] a maximum surface plasmon resonance at 520 nm obtained by UV-vis spectroscopy (Figure 23), is characteristic of colloidal AuNPs with sizes of 14.8±12 nm. Those authors studied the size dependence of the plasmon absorption of AuNPs in solution with diameters of 9, 15, 22, 48, and 99 nm, and showed that the plasmon bandwidth increased with decreasing size in the intrinsic size region (mean diameter smaller than 25 nm), but also increased with increasing size in the extrinsic size region (mean diameter larger than 25 nm).[107]

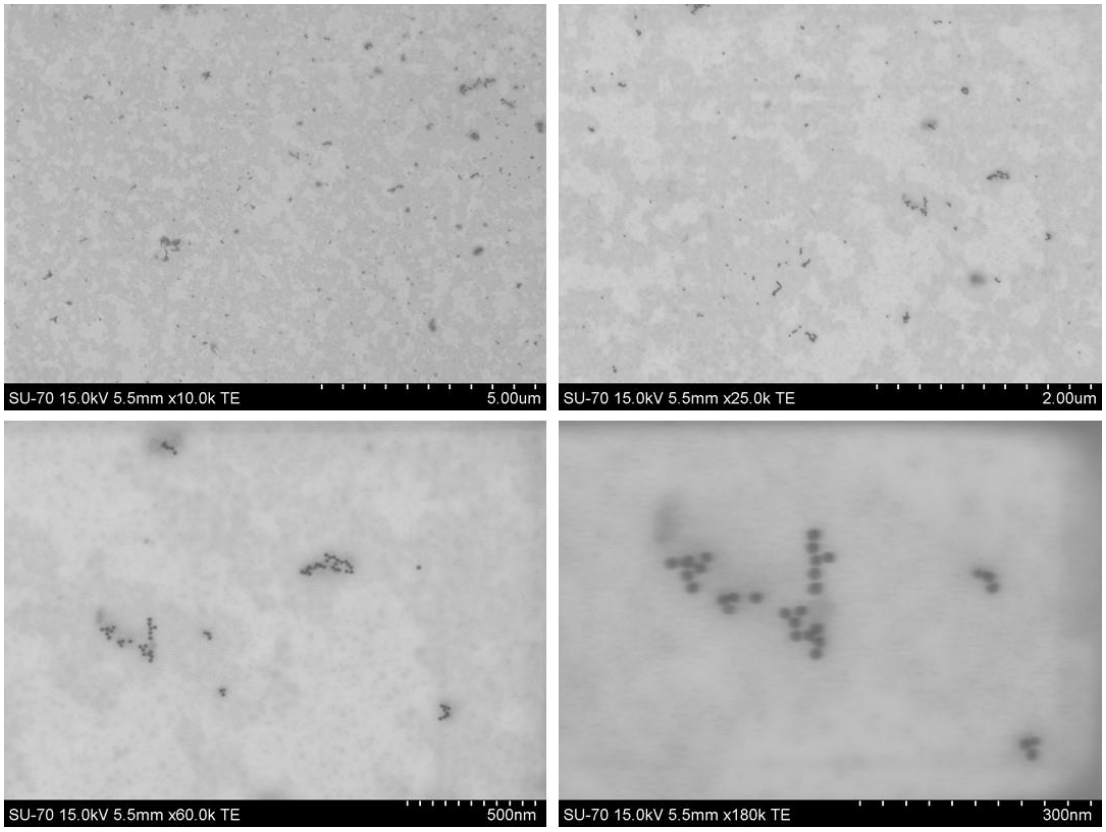

***Figure 24**. STEM micrographs of the gold nanoparticles (AuNPs).*

According to literature, there are several reports considering the use of AuNPs for thermotherapy.[108,109] For example, Lin *et al.*[110] demonstrated for the first time that spherical AuNPs of 30 nm in size conjugated with antibodies for photothermal therapy, achieving 95% cellular death rate. In a different study, Chithrani *et al.*[111] evaluated the effect of the size of AuNPs for radio-sensitization of HeLa cells. With different AuNP

sizes, ranging from 14 nm to 74 nm, the authors concluded that a size of 50 nm would result in a greater cellular intake by this cell type.

The hereby synthesized colloidal AuNPs will not be used directly as therapeutic agents,[111,112] but rather as a partner for cellulose nanobeads functionalization. In this regard, Carrick *et al.*[37] developed AuNPs functionalized cellulose beads for theranostic purposes, in which the size of the AuNPs is around 9.3 nm. Therefore, the average size of the AuNPs obtained in the present work is deemed acceptable by literature for the intended applications, although the size of the cellulose nanobeads is obviously of great importance as well, as it will dictate the cellular intake.[105]

3.3. Preparation and characterization of the cellulose nanobeads/ AuNPs hybrids

After studying the dissolution, regeneration, and hydrolysis of CA, and the synthesis of the colloidal AuNPs, the next step is dedicated to the preparation of the cellulose nanobeads/AuNPs hybrid systems, where the AuNPs will play the simultaneous role of imaging and therapeutic agent.

The cellulose nanobeads/AuNPs hybrid systems were produced via two methodologies, namely by regenerating the CA in the presence of the AuNPs followed by alkaline hydrolysis, and by performing an *in situ* synthesis of the AuNPs in the presence of the cellulose nanobeads, as summarized in Figure 25.

The ensuing cellulose nanobeads/AuNPs hybrids were characterized as regards of their optical properties by UV-vis spectroscopy, morphology and size by SEM and STEM, and elemental chemical composition by energy dispersive x-ray spectroscopy (EDS), and the advantages and limitations of the two methodologies are discussed in the following sections.

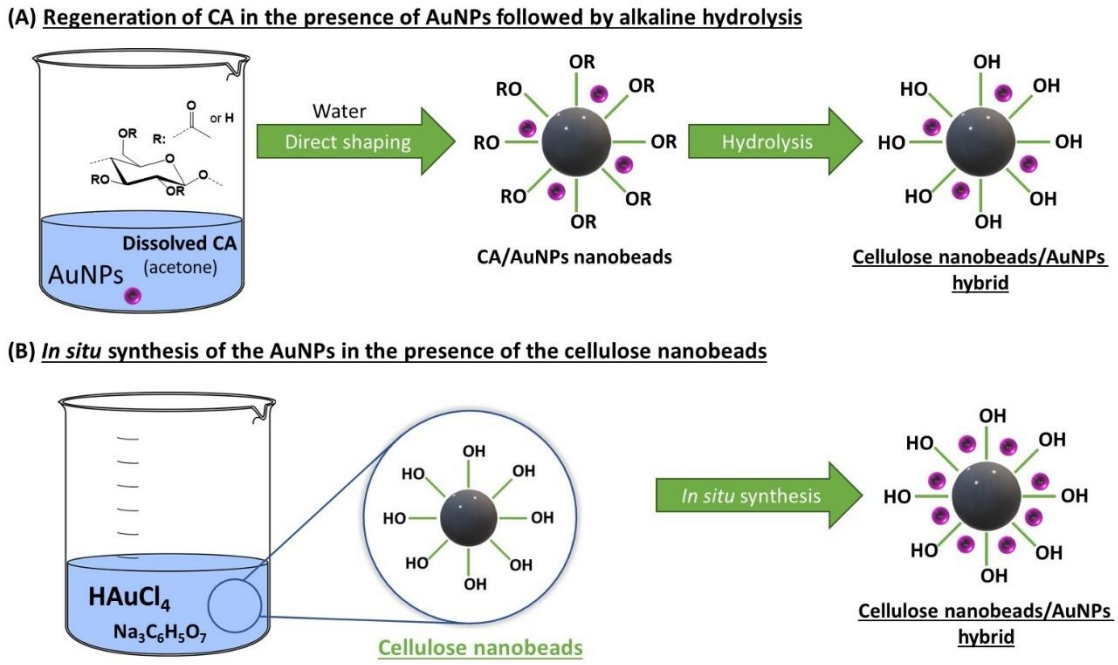

***Figure 25**. Scheme of the two methodologies followed for the functionalization of the cellulose nanobeads with AuNPs: (A) regeneration of CA in the presence of AuNPs followed by alkaline hydrolysis, and (B) in situ synthesis of the AuNPs in the presence of the cellulose nanobeads.*

3.3.1. Regeneration of CA in the presence of AuNPs followed by alkaline hydrolysis

In the first methodology (method A), the previously synthesized AuNPs were added to the CA solution in acetone, followed by regeneration via the water-on-polymer method,[98] and then the alkaline hydrolysis to obtain the cellulose nanobeads/AuNPs hybrids.

The analysis of the cellulose nanobeads/AuNPs hybrids by UV-vis spectroscopy originated an absorption spectrum (Figure 26) without any visible resonance bands. Since cellulose is well-known for not showing distinguishable UV-vis signals,[113] the non-existence of the typical SPR of AuNPs (Figure 23) indicates that there are no AuNPs at the surface of the cellulose nanobeads neither on the aqueous suspension of the cellulose nanobeads/AuNPs hybrids. This is also corroborated by the absence of the reddish color characteristic of the AuNPs, as displayed in the inset photograph (Figure 26) of the aqueous suspension of the cellulose nanobeads/AuNPs hybrid. Hence, the AuNPs are probably in the bulk of the cellulose nanobeads. Besides, the AuNPs must be

present in small amounts, otherwise they should be visible in the UV-vis spectrum, as reported by Carrick *et al*.[37] for a system of cellulose beads with encapsulated AuNPs.

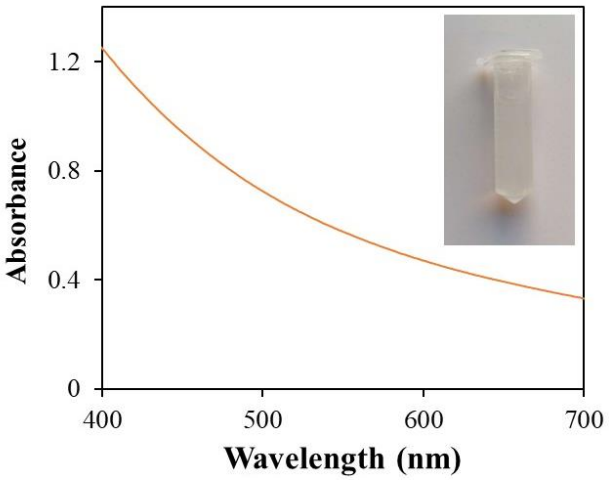

Figure 26*. UV-Vis absorption spectrum and digital photograph of the diluted aqueous suspension of cellulose nanobeads/AuNPs hybrids prepared by regenerating CA in the presence of AuNPs followed by alkaline hydrolysis.*

The morphology of the cellulose nanobeads/AuNPs hybrids was examined by SEM and STEM. According to the micrographs in Figure 27, the cellulose nanobeads/AuNPs hybrids show a spherical shape and broad size distribution with no visible evidence of AuNPs adsorbed at the surface of the cellulose nanobeads. Nevertheless, some of the nanobeads do not exhibit a smooth surface but rather reveal the existence of protuberances, bumps and holes that might be credited to the presence of AuNPs at the bulk of the cellulose nanobeads.

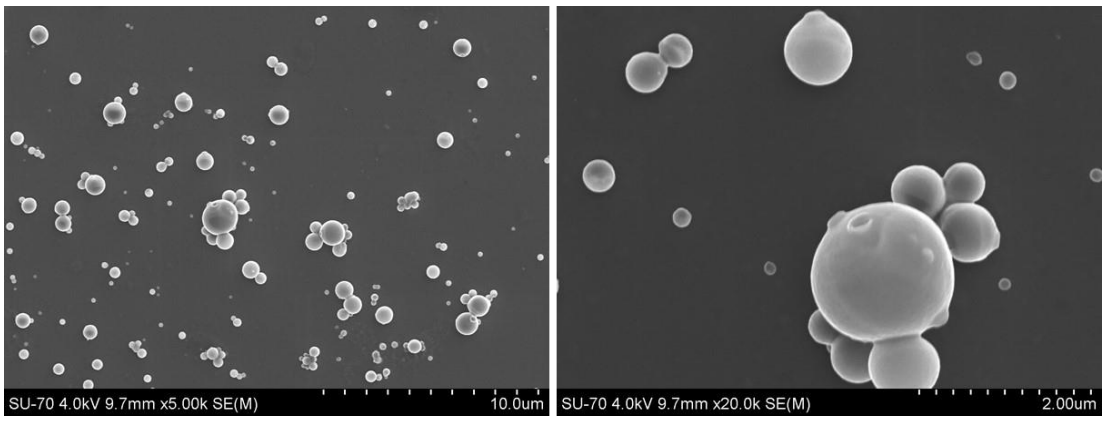

Figure 27*. SEM micrographs of the cellulose nanobeads/AuNPs hybrids prepared by regenerating CA in the presence of AuNPs followed by alkaline hydrolysis.*

On the other hand, in the STEM micrographs of Figure 28, it is possible to observe, particularly in the micrographs with higher magnifications, a few metallic nanoparticles with a very small size contrasted with the cellulose nanobeads of bigger size (see blue arrows). This validates that the AuNPs were not adsorbed at the surface but instead were incorporated in small amounts into the bulk of the cellulose nanobeads.

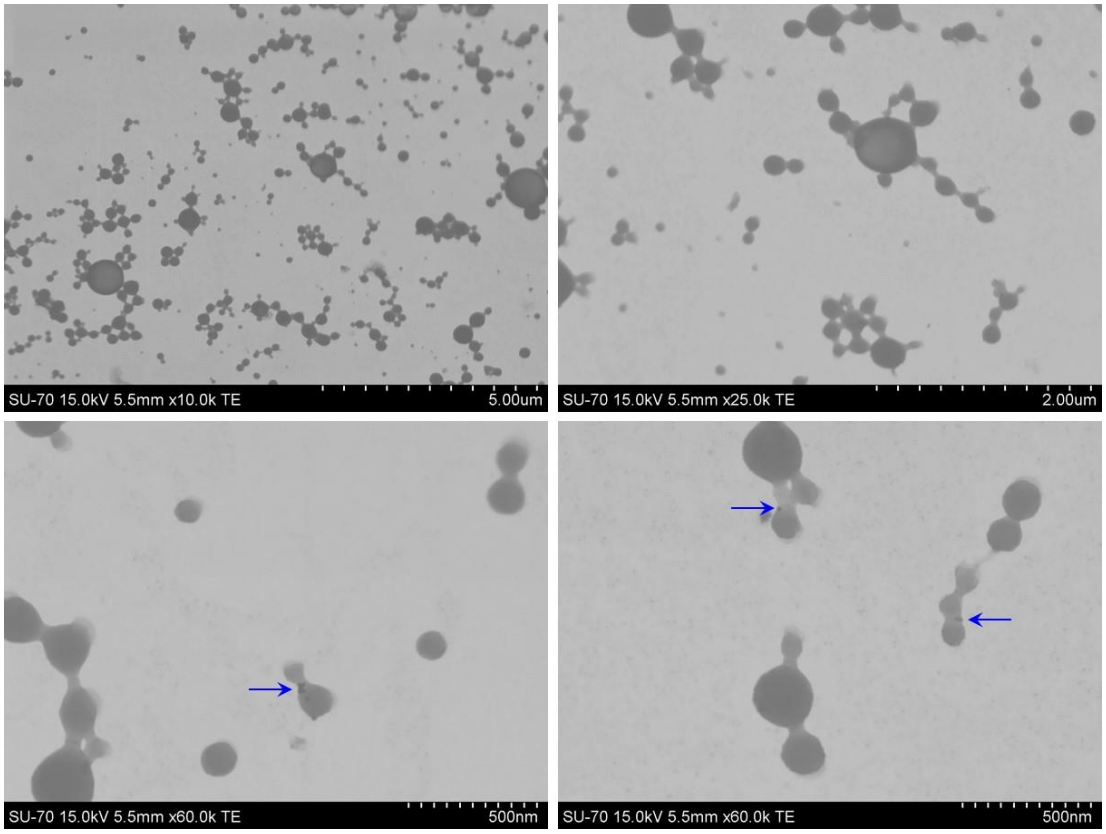

***Figure 28**. STEM micrographs of the cellulose nanobeads/AuNPs hybrids prepared by regenerating CA in the presence of AuNPs followed by alkaline hydrolysis.*

The elemental chemical composition of these cellulose nanobeads/AuNPs hybrids was evaluated by EDS analysis (Figure 29), which did not detect any gold (Au) peak. In fact, only the carbon (C), oxygen (O) and copper (Cu) peaks, assigned to cellulose nanobeads and the carbon-coated copper grid for STEM analysis, were detected in the EDS spectrum. This provides further evidence that the AuNPs are present in small amounts at the bulk of the cellulose nanobeads, in accordance with the UV-vis analysis and STEM micrographs.

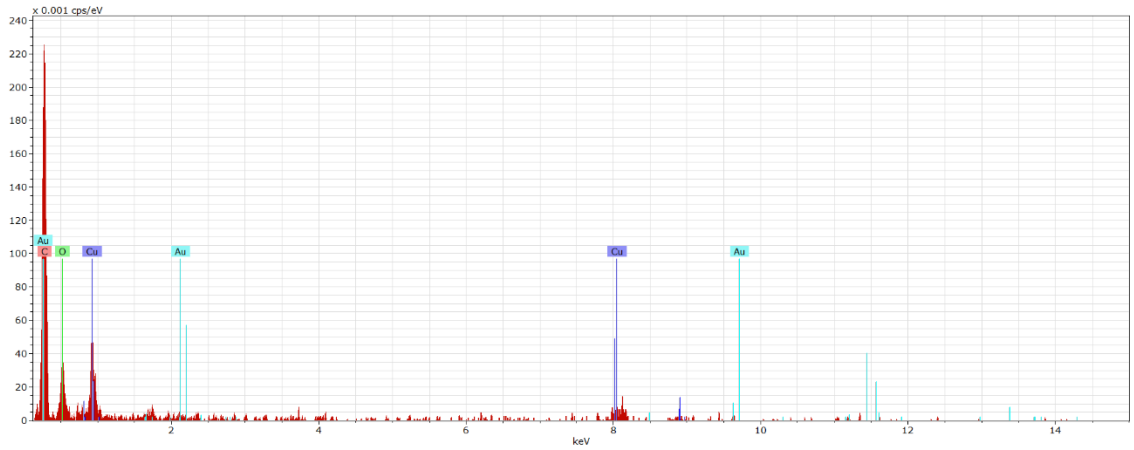

***Figure 29**. EDS spectrum of the cellulose nanobeads/AuNPs hybrids prepared by regenerating CA in the presence of AuNPs followed by alkaline hydrolysis.*

3.3.2. *In situ* synthesis of the AuNPs in the presence of the cellulose nanobeads

In the second methodology (method B), the colloidal AuNPs were synthesized in the presence of the cellulose nanobeads to produce the cellulose nanobeads/AuNPs hybrid systems. According to literature, this methodology might have an advantage when compared to the previous one.[114] In fact, when the reduction of the $[AuCl_4]^-$ complexes take place, the citrate ions are the main agents responsible for reducing $HAuCl_4$. Nevertheless, the hydroxyl groups of cellulose have been shown to provide reduction sites for the Au precursor, thus, becoming nucleation sites for the formation of Au nanoparticles, as reported in the literature.[114]

The UV-vis absorption spectrum (Figure 30) of the cellulose nanobeads/AuNPs hybrids (in dilute aqueous medium) prepared by the *in situ* synthesis of the AuNPs in the presence of the cellulose nanobeads, shows a clear SPR band at 523 nm, which is characteristic of the AuNPs, hence, confirming their presence in the hybrid system. The small shift in the resonance band when compared with the aqueous dispersion of AuNPs (without cellulose nanobeads) (Figure 23), was also reported by Majoinen *et al.*[113] for hybrid systems composed of cellulose nanocrystals and AuNPs. The presence of the AuNPs is further verified by the typical reddish color of those nanoparticles, as exhibited in the inset photograph (Figure 30) of the aqueous suspension of the cellulose nanobeads/AuNPs hybrid system.

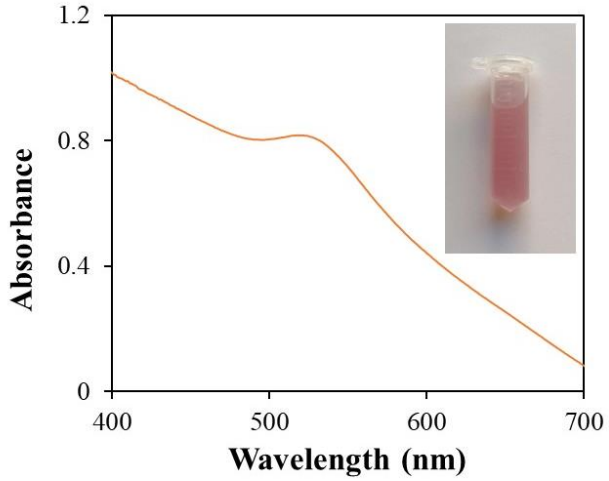

***Figure 30**. UV-Vis absorption spectrum and digital photograph of the diluted aqueous suspension of cellulose nanobeads/AuNPs hybrids prepared by the in situ synthesis of the AuNPs in the presence of the cellulose nanobeads.*

The cellulose nanobeads/AuNPs hybrids were also analyzed by SEM and STEM microscopy and the results are presented in Figure 31 and Figure 32, respectively. The micrographs obtained by both SEM and STEM depict nanobeads with a smooth surface covered with smaller nanoparticles, which, by size comparison, proved to be AuNPs. Furthermore, in the STEM micrographs (Figure 32), the metallic nanoparticles are clearly contrasted with the cellulose nanobeads. As sizes are concerned, the cellulose nanobeads exhibit a broad size distribution with an average size of 415±187 nm, while the AuNPs possess around 15±3 nm, as determined by STEM.

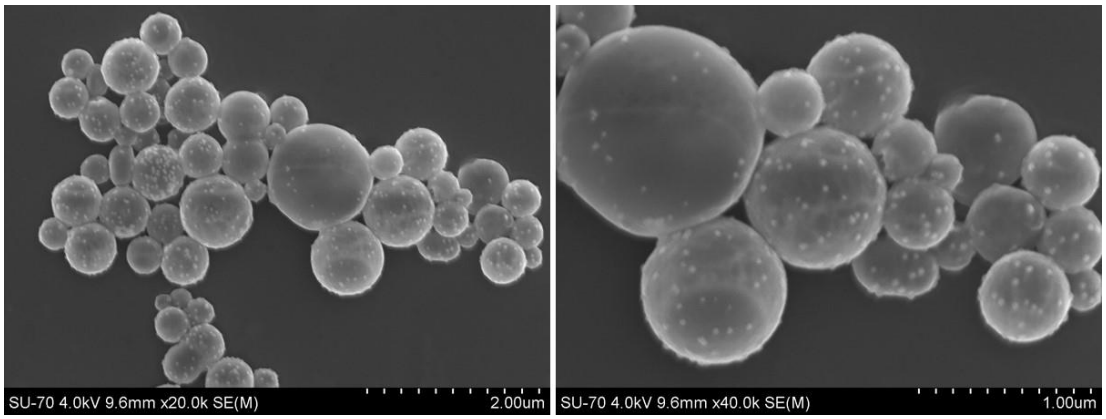

***Figure 31**. SEM micrographs of the cellulose nanobeads/AuNPs hybrids prepared by the in situ synthesis of the AuNPs in the presence of the cellulose nanobeads.*

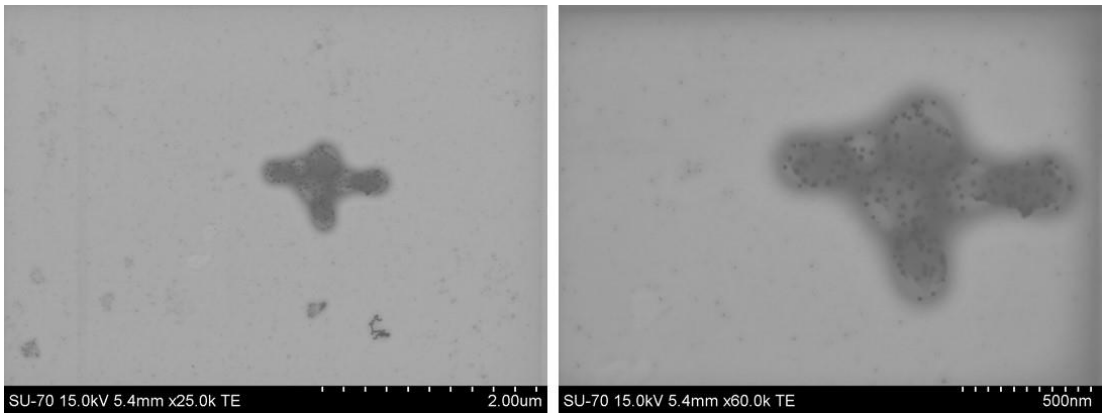

***Figure 32**. STEM micrographs of the cellulose nanobeads/AuNPs hybrids prepared by the in situ synthesis of the AuNPs in the presence of the cellulose nanobeads.*

The elemental chemical composition of the cellulose nanobeads/AuNPs hybrids, assessed by EDS analysis (Figure 33), further evidenced the presence of the AuNPs through the detection of the gold (Au) peak at 0.3, 2.1 and 9.7 keV.[115] The other peaks, namely the carbon (C) peak at 0.27 keV and the oxygen (O) peak at 0.51 keV, are assigned to the cellulose nanobeads, while the copper (Cu) peaks at 0.9 and 8.0 keV are allocated to the carbon-coated copper grid for STEM analysis.

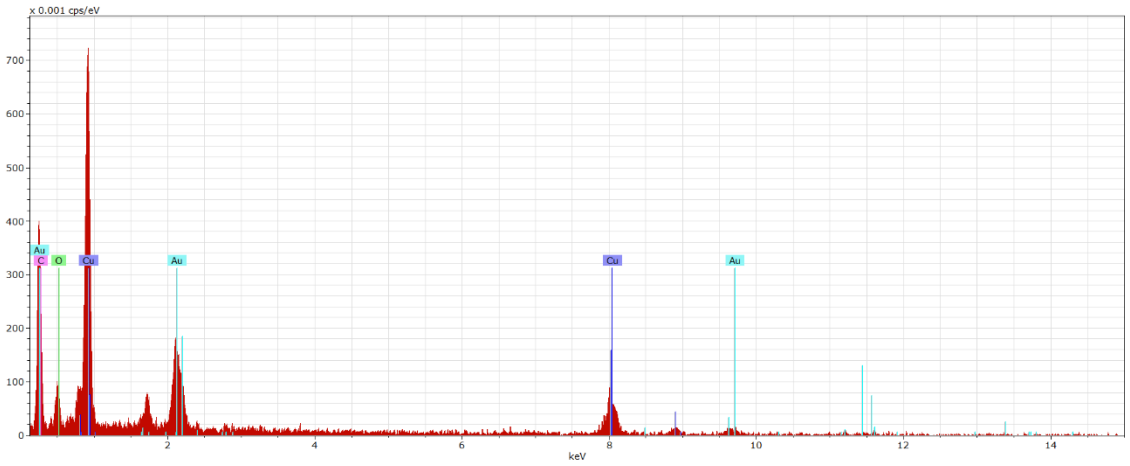

***Figure 33**. EDS spectrum of the cellulose nanobeads/AuNPs hybrids prepared by the in situ synthesis of the AuNPs in the presence of the cellulose nanobeads.*

From these results, it is evident that this second methodology was more successful than the first methodology, where the cellulose nanobeads/AuNPs hybrids were prepared by regenerating CA in the presence of AuNPs followed by alkaline hydrolysis. In fact, following the second methodology, it was possible to confirm the

presence of the AuNPs at the surface of the cellulose nanobeads by the color change, UV-vis spectroscopy, SEM, STEM, and EDS. Hence, the cellulose nanobeads/AuNPs hybrids prepared by the *in situ* synthesis of the AuNPs in the presence of the cellulose nanobeads were selected to assess their behavior towards cancer cells, as examined in the following section.

When compared with other cellulose/AuNPs systems, the cellulose nanobeads/AuNPs hybrids developed in the present study exhibit a higher average size than, for instance, the system developed by Carrick *et al.*[37] consisting of cellulose beads (160−170 nm) with encapsulated AuNPs (9.3 nm). Although sizes lower than 200 nm are preferred for nanomedical applications,[116,117] the obtained size for the cellulose nanobeads/AuNPs hybrid systems (cellulose nanobeads: 415±187 nm, AuNPs: 15±3 nm) is also considered acceptable for the intended application.[118] In fact, there are examples in literature where systems with sizes around 400-500 nm have been used, as discussed in the appraisals by Morales-Cruz *et al.*[119] about the smart targeting to improve cancer therapeutics, and by Rie and Thielemans[105] regarding the state-of-the-art on cellulose/gold nanoparticle hybrid materials.

3.4. *In vitro* cytotoxicity of the cellulose nanobeads/AuNPs hybrids

The *in vitro* cytotoxicity of the cellulose nanobeads/AuNPs hybrids was evaluated by the MTT (3-[4,5-dimethylthiazol-2-yl]-2,5-diphenyltetrazolium bromide) assay towards the pigmented human melanoma (MNT-1) cell line. The MTT essay is a colorimetric test based on the conversion of the water-soluble tetrazolium salt, *i.e.*, MTT, into a purple-colored formazan by viable cells (Figure 34), and the amount of formazan is used for the quantification of the cell metabolic activity.[121] The MNT-1 cell line was chosen because previous studies have demonstrated that AuNPs induce cell death and suppress migration of melanoma cells.[120]

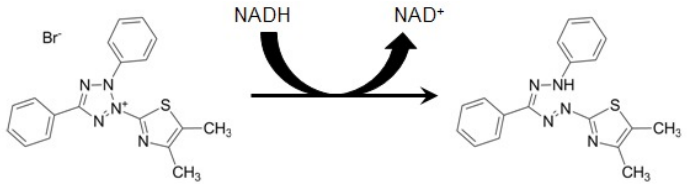

***Figure 34**. Metabolic conversion of the water soluble MTT to the insoluble formazan.*[121]

Herein, the MNT-1 cells were exposed to the cellulose nanobeads with and without AuNPs at different concentrations, namely 4.9, 9.8, 19.5 and 39.0 μg mL^{-1}, during 24 h. The obtained results for the 24-hours MTT assay are depicted in Figure 35, and clearly show that the cellulose nanobeads are non-cytotoxic towards MNT-1 cells up to concentrations of 39.0 μg mL^{-1}, with a cell viability of *ca*. 100%. This was anticipated because cellulose is a polysaccharide that does not cause cellular toxicity neither exhibits anticancer activity.[122]

Conversely, the cellulose nanobeads/AuNPs hybrid system presented a dose-dependent cellular toxicity, reaching a cell viability of 81.6±4.5% at a concentration of 39.0 μg mL^{-1}. This coherent decline of the MNT-1 cell viability while increasing the concentration of the cellulose nanobeads/AuNPs hybrid system from 4.9 μg mL^{-1} to 39.0 μg mL^{-1}, suggests that higher doses (> 39.0 μg mL^{-1}) will promote a higher cell viability reduction towards the melanoma cells. Hence, this cytotoxic effect is most definitely credited to the AuNPs, which is in agreement with the ability of these colloidal nanoparticles to induce cell death and suppress migration of melanoma cells.[120]

Despite the promising results obtained for the 24-hour MTT assay, other concentrations (*e.g.*, 50, 100, 150 and 200 μg mL^{-1}) and exposure times (*e.g.*, 48 and 72 h) should be performed in order to prove, without a doubt, that the cellulose nanobeads/AuNPs hybrid system possesses antitumoral activity.

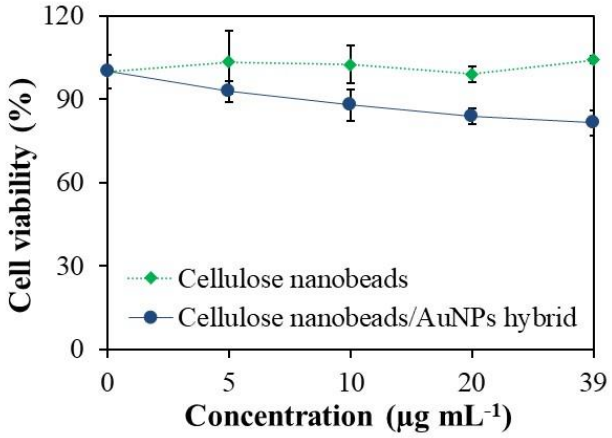

Figure 35. *Cell viability of the MNT-1 cells determined by the MTT assay after 24 h exposure to cellulose nanobeads and cellulose nanobeads/AuNPs hybrid.*

CHAPTER 4 – CONCLUSIONS AND FUTURE WORK

The present work aimed at developing multifunctional cellulose nanobeads for potential application on the diagnosis and treatment of cancer. From the accomplished results, it was possible to conclude that cellulose diacetate, a non-toxic, and biodegradable cellulose ester applied in the biomedical field, can be dissolved using acetone, and subsequently regenerated into nanobeads using water as the non-solvent through the nanoprecipitation method. The produced nanobeads show a spherical shape with an average size of 456±185 nm. Furthermore, the alkaline hydrolysis of the regenerated CA nanobeads was confirmed by infrared spectroscopy, demonstrating the removal of some of the acetyl groups available at the surface of the nanobeads, and the SEM micrographs supported that the cellulose nanobeads preserved their spherical shape and size.

Subsequently, hybrid systems composed of cellulose nanobeads and AuNPs were prepared by two distinct methodologies, namely by regenerating the CA in the presence of the AuNPs followed by alkaline hydrolysis and by performing an *in situ* synthesis of the AuNPs in the presence of the cellulose nanobeads (Figure 25). Overall, the results demonstrated that the second methodology was the successful one, because it was possible to confirm the presence of the AuNPs at the surface of the cellulose nanobeads by the color change, UV-vis spectroscopy, SEM, STEM, and EDS.

The morphology and size of the hybrid systems were evaluated by SEM and STEM, which confirmed the production of the cellulose nanobeads/AuNPs hybrids with an average size of 415±187 nm for the cellulose nanobeads and 15±3 nm for the AuNPs. Moreover, the *in vitro* cytotoxicity of the cellulose nanobeads/AuNPs hybrids towards pigmented human melanoma (MNT-1) cell line was evaluated and the data showed that the hybrid system exhibits a dose-dependent cellular toxicity. When the cells were exposed to 39.0 μg mL^{-1} of hybrid for 24 h, the cell viability was reduced to 81.6±4.5%. Thus, the augment of the hybrid concentration will certainly translate into antitumoral activity.

The all-inclusive findings support the potential of the developed cellulose nanobeads/AuNPs hybrids for applications in cell imaging and thermotherapy for the diagnosis and treatment of cancer.

Among the possible lines of future work, it would be interesting to pursue the topics summarized in Figure 36, to increase the potential of the cellulose nanobeads/AuNPs hybrid systems in what concerns: (i) the addition of targeting agents for improved cellular uptake, (ii) the loading of anticancer drugs for multimodal synergistic therapy, (iii) the evaluation of the *in vitro* cytotoxicity, cellular uptake and photothermal ablation of cancer cells, and (iv) the development of advanced self-propelled motile systems.

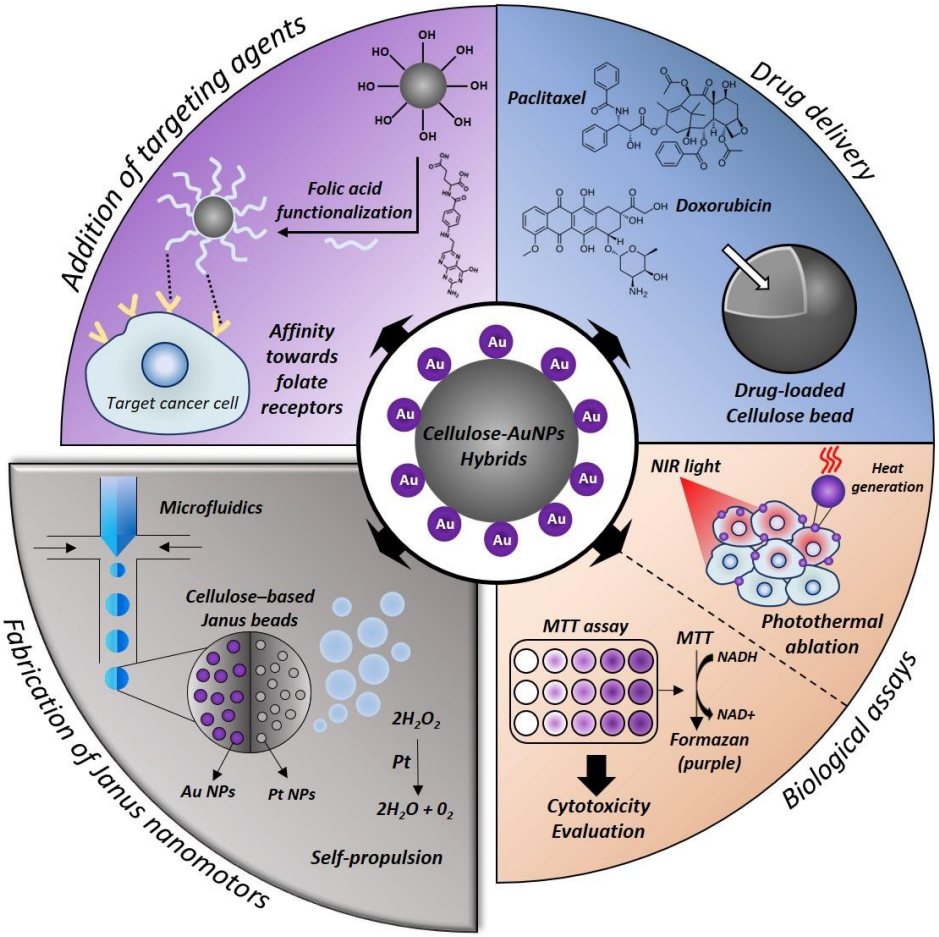

***Figure 36**. Schematic representation of future work proposals for the cellulose nanobeads/AuNPs hybrid systems.*

The cellulose nanobeads/AuNPs hybrid systems developed here can be enhanced towards the intended application, through the incorporation of a targeting agent. In fact, the addition of ligands that possess targeting affinity to cancer cell specific markers greatly increases their efficiency. For instance, some types of cancer,

namely breast, ovarian, lung, kidney, brain, and endometrial cancer, possess overexpressed folate receptors that mediate the cellular intake of folic acid, while normal tissues rarely express these receptors.[123] Therefore, the functionalization of the cellulose nanobeads/AuNPs hybrids with folic acid, would be a possible strategy to augment their target affinity to cancer cells and improve cellular uptake.

As discussed in the bibliographic review section (Chapter 1), the multimodal synergistic therapy is currently one of the best approaches for cancer treatment.[9] In this perspective, the present cellulose nanobeads/AuNPs hybrid systems have potential for the encapsulation and release of anticancer drugs (*e.g.*, doxorubicin, paclitaxel), alongside the inherent cytotoxic effect associated with the AuNPs. Furthermore, photothermal therapy against cancer cells can also be employed through AuNPs, which is made possible by their unique surface plasmon resonance features. Briefly, upon receiving near infra-red radiation, the free electrons of AuNPs are excited, originating collective oscillation. This, in turn, releases thermal energy to the surrounding medium that can be used to ablate cancer cells.[124] The theoretical synergy resulting from these different kinds of therapy would greatly improve the chance of successfully killing tumour cells.[125]

Additionally, these cellulose nanobeads/AuNP hybrid systems can be the starting point for the development of advanced motile tools, namely nanomotors (Figure 36), which are essentially self-propelling nanoparticles with the ability to convert energy into motion, and, thus, can propel themselves to a target with elevated precision.[126] Among the available methodologies to develop such micro and nanomachines, the microfluidics technology allows the precise control over multiple phases of fluids in restricted and integrated microchannels, allowing the creation of small particles with distinct shapes and structures, such as the Janus particles.[127] These were named after the double-faced roman god Janus, and have recently surfaced as a new division of colloidal structures, that exhibit distinct architectural features with two sides or two surfaces with different chemistry and/or polarity. The absence of centrosymmetry in the Janus particles has revealed novel properties regarding peculiar aggregation behaviour and formation of superstructures of different sizes, with potential for medicine, physics, biochemistry, and colloidal chemistry applications. Due to the anisotropic surface characteristics and multifunctionality provided from their tunable asymmetric structure, Janus particles optimistically satisfy the conditions to act as nanomotors.[128,129]

When compared with traditional nanoparticle systems, nanomotors possess the advantage of actively targeting a specific biological environment with the aid of a propulsion mechanism, whereas in the absence of driving forces, the passive transportation of therapeutic compounds is not as effective.[126] In fact, although major breakthroughs have been achieved in this regard, effective passage of passive particles into cells still constitutes a crucial limitation to intra-cellular treatments, as nanoparticles lack the strength to overcome biological barriers, cell-nanoparticle interactions, off-target accumulations, and restricted motion control inside cells.[130,131]

In the scope of the present study, the idea here would be to engineer spherical Janus nanomotors consisting of cellulose, AuNPs and platinum nanoparticles. The latter component will act as a catalyst for the decomposition of hydrogen peroxide, which in turn produces oxygen bubbles that serve to propel the nanomotor.[132] Overall, adding nanomotor functionality to the cellulose nanobeads/AuNPs hybrids through Janus structures achieved by microfluidics, would represent a great advantage for overcoming the biological barriers in pursuit of its target, the cancer cells.[130,131]

REFERENCES

(1) Peer, D.; Karp, J. M.; Hong, S.; Farokhzad, O. C.; Margalit, R.; Langer, R. Nanocarriers as an Emerging Platform for Cancer Therapy. *Nat. Nanotechnol.* **2007**, *2* (12), 751–760. https://doi.org/10.1038/nnano.2007.387.

(2) Senapati, S.; Mahanta, A. K.; Kumar, S.; Maiti, P. Controlled Drug Delivery Vehicles for Cancer Treatment and Their Performance. *Signal Transduct. Target. Ther.* **2018**, *3* (1), 7. https://doi.org/10.1038/s41392-017-0004-3.

(3) Bahrami, B.; Hojjat-Farsangi, M.; Mohammadi, H.; Anvari, E.; Ghalamfarsa, G.; Yousefi, M.; Jadidi-Niaragh, F. Nanoparticles and Targeted Drug Delivery in Cancer Therapy. *Immunol. Lett.* **2017**, *190* (April), 64–83. https://doi.org/10.1016/j.imlet.2017.07.015.

(4) Cho, K.; Wang, X.; Nie, S.; Chen, Z.; Shin, D. M. Therapeutic Nanoparticles for Drug Delivery in Cancer. *Clin. Cancer Res.* **2008**, *14* (5), 1310–1316. https://doi.org/10.1158/1078-0432.CCR-07-1441.

(5) Fathi, M.; Abdolahinia, E. D.; Barar, J.; Omidi, Y. Smart Stimuli-Responsive Biopolymeric Nanomedicines for Targeted Therapy of Solid Tumors. *Nanomedicine* **2020**, *15* (22), 2171–2200. https://doi.org/10.2217/nnm-2020-0146.

(6) Chivere, V. T.; Kondiah, P. P. D.; Choonara, Y. E.; Pillay, V. Nanotechnology-Based Biopolymeric Oral Delivery Platforms for Advanced Cancer Treatment. *Cancers (Basel).* **2020**, *12* (2), 522. https://doi.org/10.3390/cancers12020522.

(7) Halib, N.; Perrone, F.; Id, M. C.; Dapas, B.; Farra, R.; Abrami, M.; Chiarappa, G.; Forte, G.; Zanconati, F.; Pozzato, G.; Murena, L.; Fiotti, N.; Lapasin, R.; Cansolino, L.; Grassi, G.; Id, M. G. Potential Applications of Nanocellulose-Containing Materials in the Biomedical Field. *Materials (Basel).* **2017**, *10* (8), 977. https://doi.org/10.3390/ma10080977.

(8) Feldman, D. Polymers and Polymer Nanocomposites for Cancer Therapy. *Appl. Sci.* **2019**, *9* (18), 3899. https://doi.org/10.3390/app9183899.

(9) Fan, W.; Yung, B.; Huang, P.; Chen, X. Nanotechnology for Multimodal Synergistic Cancer Therapy. *Chem. Rev.* **2017**, *117* (22), 13566–13638. https://doi.org/10.1021/acs.chemrev.7b00258.

(10) Park, S.; Aalipour, A.; Vermesh, O.; Yu, J. H.; Gambhir, S. S. Towards Clinically Translatable *in vivo* Nanodiagnostics. *Nat. Rev. Mater.* **2017**, *2* (5), 17014. https://doi.org/10.1038/natrevmats.2017.14.

(11) Zhang, Y.; Li, M.; Gao, X.; Chen, Y.; Liu, T. Nanotechnology in Cancer Diagnosis: Progress, Challenges and Opportunities. *J. Hematol. Oncol.* **2019**, *12* (1), 137. https://doi.org/10.1186/s13045-019-0833-3.

(12) Yoon, Y. Il; Tang, W.; Chen, X. Ultrasound-Mediated Diagnosis and Therapy Based on Ultrasound Contrast Agents. *Small Methods* **2017**, *1* (8), 1700173. https://doi.org/10.1002/smtd.201700173.

(13) Kim, C.; Favazza, C.; Wang, L. V. *In vivo* Photoacoustic Tomography of Chemicals: High-Resolution Functional and Molecular Optical Imaging at New Depths. *Chem. Rev.* **2010**, *110* (5), 2756–2782. https://doi.org/10.1021/cr900266s.

(14) Gao, X.; Cui, Y.; Levenson, R. M.; Chung, L. W. K.; Nie, S. *In vivo* Cancer Targeting and Imaging with Semiconductor Quantum Dots. *Nat. Biotechnol.* **2004**, *22* (8), 969–976. https://doi.org/10.1038/nbt994.

(15) Goulart, B. H. L.; Bensink, M. E.; Mummy, D. G.; Ramsey, S. D. Lung Cancer Screening With Low-Dose Computed Tomography: Costs, National Expenditures, and Cost-Effectiveness. *J. Natl. Compr. Cancer Netw.* **2012**, *10* (2), 267–275. https://doi.org/10.6004/jnccn.2012.0023.

(16) Gambhir, S. S. Molecular Imaging of Cancer with Positron Emission Tomography. *Nat. Rev. Cancer* **2002**, *2* (9), 683–693. https://doi.org/10.1038/nrc882.

(17) Frangioni, J. V. New Technologies for Human Cancer Imaging. *J. Clin. Oncol.* **2008**, *26* (24), 4012–4021. https://doi.org/10.1200/JCO.2007.14.3065.

(18) Ehlerding, E. B.; Grodzinski, P.; Cai, W.; Liu, C. H. Big Potential from Small Agents: Nanoparticles for Imaging-Based Companion Diagnostics. *ACS Nano* **2018**, *12* (3), 2106–2121. https://doi.org/10.1021/acsnano.7b07252.

(19) Tran, S.; DeGiovanni, P.-J.; Piel, B.; Rai, P. Cancer Nanomedicine: A Review of Recent Success in Drug Delivery. *Clin. Transl. Med.* **2017**, *6* (1). https://doi.org/10.1186/s40169-017-0175-0.

(20) Danhier, F.; Feron, O.; Préat, V. To Exploit the Tumor Microenvironment: Passive and Active Tumor Targeting of Nanocarriers for Anti-Cancer Drug Delivery. *J. Control. Release* **2010**, *148* (2), 135–146.

https://doi.org/10.1016/j.jconrel.2010.08.027.

(21) Petros, R. A.; DeSimone, J. M. Strategies in the Design of Nanoparticles for Therapeutic Applications. *Nat. Rev. Drug Discov.* **2010**, *9* (8), 615–627. https://doi.org/10.1038/nrd2591.

(22) Shi, J.; Kantoff, P. W.; Wooster, R.; Farokhzad, O. C. Cancer Nanomedicine: Progress, Challenges and Opportunities. *Nat. Rev. Cancer* **2017**, *17* (1), 20–37. https://doi.org/10.1038/nrc.2016.108.

(23) Karimian, A.; Parsian, H.; Majidinia, M.; Rahimi, M.; Mir, S. M.; Samadi Kafil, H.; Shafiei-Irannejad, V.; Kheyrollah, M.; Ostadi, H.; Yousefi, B. Nanocrystalline Cellulose: Preparation, Physicochemical Properties, and Applications in Drug Delivery Systems. *Int. J. Biol. Macromol.* **2019**, *133*, 850–859. https://doi.org/10.1016/j.ijbiomac.2019.04.117.

(24) Ferrari, M. Cancer Nanotechnology: Opportunities and Challenges. *Nat. Rev. Cancer* **2005**, *5* (3), 161–171. https://doi.org/10.1038/nrc1566.

(25) Farokhzad, O. C.; Langer, R. Impact of Nanotechnology on Drug Delivery. *ACS Nano* **2009**, *3* (1), 16–20. https://doi.org/10.1021/nn900002m.

(26) Au, J. L. S.; Yeung, B. Z.; Wientjes, M. G.; Lu, Z.; Wientjes, M. G. Delivery of Cancer Therapeutics to Extracellular and Intracellular Targets: Determinants, Barriers, Challenges and Opportunities. *Adv. Drug Deliv. Rev.* **2016**, *97*, 280–301. https://doi.org/10.1016/j.addr.2015.12.002.

(27) Sharma, S. K.; Shrivastava, N.; Rossi, F.; Tung, L. D.; Thanh, N. T. K. Nanoparticles-Based Magnetic and Photo Induced Hyperthermia for Cancer Treatment. *Nano Today* **2019**, *29* (xxxx), 100795. https://doi.org/10.1016/j.nantod.2019.100795.

(28) Yang, X.; Gao, L.; Guo, Q.; Li, Y.; Ma, Y.; Yang, J.; Gong, C.; Yi, C. Nanomaterials for Radiotherapeutics-Based Multimodal Synergistic Cancer Therapy. *Nano Res.* **2020**, *13* (10), 2579–2594. https://doi.org/10.1007/s12274-020-2722-z.

(29) Davis, M. E.; Chen, Z.; Shin, D. M. Nanoparticle Therapeutics: An Emerging Treatment Modality for Cancer. *Nat. Rev. Drug Discov.* **2008**, *7* (9), 771–782. https://doi.org/10.1038/nrd2614.

(30) Blanco, E.; Shen, H.; Ferrari, M. Principles of Nanoparticle Design for Overcoming Biological Barriers to Drug Delivery. *Nat. Biotechnol.* **2015**, *33* (9), 941–951. https://doi.org/10.1038/nbt.3330.

(31) Zhang, R.; Cheng, K.; Antaris, A. L.; Ma, X.; Yang, M.; Ramakrishnan, S.; Liu, G.; Lu, A.; Dai, H.; Tian, M.; Cheng, Z. Hybrid Anisotropic Nanostructures for Dual-Modal Cancer Imaging and Image-Guided Chemo-Thermo Therapies. *Biomaterials* **2016**, *103*, 265–277. https://doi.org/10.1016/j.biomaterials.2016.06.063.

(32) Chen, G.; Roy, I.; Yang, C.; Prasad, P. N. Nanochemistry and Nanomedicine for Nanoparticle-Based Diagnostics and Therapy. *Chem. Rev.* **2016**, *116* (5), 2826–2885. https://doi.org/10.1021/acs.chemrev.5b00148.

(33) Garland, N. T.; McLamore, E. S.; Gomes, C.; Marrow, E. A.; Daniele, M. A.; Walper, S.; Medintz, I. L.; Claussen, J. C. Synthesis and Applications of Cellulose Nanohybrid Materials. In *Hybrid Polymer Composite Materials*; Elsevier, 2017; pp 289–320. https://doi.org/10.1016/B978-0-08-100785-3.00010-3.

(34) Guo, R.; Huang, F.; Zhang, B.; Yan, Y.; Che, J.; Jin, Y.; Zhuang, Y.; Dong, R.; Li, Y.; Tan, B.; Song, R.; Hu, Y.; Dong, X.; Li, X.; Lin, N. GSH Activated Biotin-Tagged Near-Infrared Probe for Efficient Cancer Imaging. *Theranostics* **2019**, *9* (12), 3515–3525. https://doi.org/10.7150/thno.32742.

(35) Ayub, A. D.; Chiu, H. I.; Mat Yusuf, S. N. A.; Abd Kadir, E.; Ngalim, S. H.; Lim, V. Biocompatible Disulphide Cross-Linked Sodium Alginate Derivative Nanoparticles for Oral Colon-Targeted Drug Delivery. *Artif. Cells, Nanomedicine, Biotechnol.* **2019**, *47* (1), 353–369. https://doi.org/10.1080/21691401.2018.1557672.

(36) Mura, S.; Nicolas, J.; Couvreur, P. Stimuli-Responsive Nanocarriers for Drug Delivery. *Nat. Mater.* **2013**, *12* (11), 991–1003. https://doi.org/10.1038/nmat3776.

(37) Carrick, C.; Wågberg, L.; Larsson, P. A. Immunoselective Cellulose Nanospheres: A Versatile Platform for Nanotheranostics. *ACS Macro Lett.* **2014**, *3* (11), 1117–1120. https://doi.org/10.1021/mz500507k.

(38) Rosenblum, D.; Joshi, N.; Tao, W.; Karp, J. M.; Peer, D. Progress and Challenges towards Targeted Delivery of Cancer Therapeutics. *Nat. Commun.* **2018**, *9* (1), 1410. https://doi.org/10.1038/s41467-018-03705-y.

(39) Pearce, A. K.; O'Reilly, R. K. Insights into Active Targeting of Nanoparticles in Drug Delivery: Advances in Clinical Studies and Design Considerations for Cancer Nanomedicine. *Bioconjug. Chem.* **2019**, *30* (9), 2300–2311.

https://doi.org/10.1021/acs.bioconjchem.9b00456.

(40) Lu, Y.; Aimetti, A. A.; Langer, R.; Gu, Z. Bioresponsive Materials. *Nat. Rev. Mater.* **2017**, *2* (1), 16075. https://doi.org/10.1038/natrevmats.2016.75.

(41) Ageitos, J. M.; Chuah, J. A.; Numata, K. Design Considerations for Properties of Nanocarriers on Disposition and Efficiency of Drug and Gene Delivery. *RSC Drug Discov. Ser.* **2016**, *2016-Janua* (51), 1–22. https://doi.org/10.1039/9781782622536-00001.

(42) Gao, S.; Tang, G.; Hua, D.; Xiong, R.; Han, J.; Jiang, S.; Zhang, Q.; Huang, C. Stimuli-Responsive Bio-Based Polymeric Systems and Their Applications. *J. Mater. Chem. B* **2019**, *7* (5), 709–729. https://doi.org/10.1039/C8TB02491J.

(43) Talebian, S.; Foroughi, J.; Wade, S. J.; Vine, K. L.; Dolatshahi-Pirouz, A.; Mehrali, M.; Conde, J.; Wallace, G. G. Biopolymers for Antitumor Implantable Drug Delivery Systems: Recent Advances and Future Outlook. *Adv. Mater.* **2018**, *30* (31), 1706665. https://doi.org/10.1002/adma.201706665.

(44) Rojas, O.; Bedoya, M.; Yhors, C. Current Trends in the Production of Cellulose Nanoparticles and Nanocomposites for Biomedical Applications. In *Cellulose - Fundamental Aspects and Current Trends*; IntechOpen, 2015; pp 194–228. https://doi.org/10.5772/61334.

(45) Jacob, J.; Haponiuk, J. T.; Thomas, S.; Gopi, S. Biopolymer Based Nanomaterials in Drug Delivery Systems: A Review. *Mater. Today Chem.* **2018**, *9*, 43–55. https://doi.org/10.1016/j.mtchem.2018.05.002.

(46) Ching, S. H.; Bansal, N.; Bhandari, B. Alginate Gel Particles–A Review of Production Techniques and Physical Properties. *Crit. Rev. Food Sci. Nutr.* **2017**, *57* (6), 1133–1152. https://doi.org/10.1080/10408398.2014.965773.

(47) Seib, F. P.; Jones, G. T.; Rnjak-Kovacina, J.; Lin, Y.; Kaplan, D. L. PH-Dependent Anticancer Drug Release from Silk Nanoparticles. *Adv. Healthc. Mater.* **2013**, *2* (12), 1606–1611. https://doi.org/10.1002/adhm.201300034.

(48) Ma, Y.; Canup, B. S. B.; Tong, X.; Dai, F.; Xiao, B. Multi-Responsive Silk Fibroin-Based Nanoparticles for Drug Delivery. *Front. Chem.* **2020**, *8* (November), 1–5. https://doi.org/10.3389/fchem.2020.585077.

(49) Ali, A.; Ahmed, S. A Review on Chitosan and Its Nanocomposites in Drug Delivery. *Int. J. Biol. Macromol.* **2018**, *109*, 273–286. https://doi.org/10.1016/j.ijbiomac.2017.12.078.

(50) Barbieri, S.; Buttini, F.; Rossi, A.; Bettini, R.; Colombo, P.; Ponchel, G.;

Sonvico, F.; Colombo, G. Ex Vivo Permeation of Tamoxifen and Its 4-OH Metabolite through Rat Intestine from Lecithin/Chitosan Nanoparticles. *Int. J. Pharm.* **2015**, *491* (1–2), 99–104. https://doi.org/10.1016/j.ijpharm.2015.06.021.

(51) Rojas, O. J. *Cellulose Chemistry and Properties: Fibers, Nanocelluloses and Advanced Materials*; Rojas, O. J., Ed.; Advances in Polymer Science; Springer International Publishing: Cham, 2016; Vol. 271. https://doi.org/10.1007/978-3-319-26015-0.

(52) Tian, H.; He, J. Cellulose as a Scaffold for Self-Assembly: From Basic Research to Real Applications. *Langmuir* **2016**, *32* (47), 12269–12282. https://doi.org/10.1021/acs.langmuir.6b02033.

(53) Habibi, Y.; Lucia, L. A.; Rojas, O. J. Cellulose Nanocrystals: Chemistry, Self-Assembly, and Applications. *Chem. Rev.* **2010**, *110* (6), 3479–3500. https://doi.org/10.1021/cr900339w.

(54) Moon, R. J.; Martini, A.; Nairn, J.; Simonsen, J.; Youngblood, J. Cellulose Nanomaterials Review: Structure, Properties and Nanocomposites. *Chem. Soc. Rev.* **2011**, *40* (7), 3941. https://doi.org/10.1039/c0cs00108b.

(55) Wang, S.; Lu, A.; Zhang, L. Recent Advances in Regenerated Cellulose Materials. *Prog. Polym. Sci.* **2016**, *53*, 169–206. https://doi.org/10.1016/j.progpolymsci.2015.07.003.

(56) Abitbol, T.; Rivkin, A.; Cao, Y.; Nevo, Y.; Abraham, E.; Ben-Shalom, T.; Lapidot, S.; Shoseyov, O. Nanocellulose, a Tiny Fiber with Huge Applications. *Curr. Opin. Biotechnol.* **2016**, *39* (I), 76–88. https://doi.org/10.1016/j.copbio.2016.01.002.

(57) Khine, Y. Y.; Stenzel, M. H. Surface Modified Cellulose Nanomaterials: A Source of Non-Spherical Nanoparticles for Drug Delivery. *Mater. Horizons* **2020**, *7* (7), 1727–1758. https://doi.org/10.1039/C9MH01727E.

(58) Gupta, P. K.; Raghunath, S. S.; Prasanna, D. V.; Venkat, P.; Shree, V.; Chithananthan, C.; Choudhary, S.; Surender, K.; Geetha, K. An Update on Overview of Cellulose, Its Structure and Applications. In *Cellulose*; IntechOpen, 2019. https://doi.org/10.5772/intechopen.84727.

(59) Kim, J.; Zhai, L.; Mun, S.; Ko, H.-U.; Yun, Y.-M. Cellulose Nanocrystals, Nanofibers, and Their Composites as Renewable Smart Materials. In *Nanosensors, Biosensors, and Info-Tech Sensors and Systems 2015*; Varadan, V. K., Ed.; 2015; Vol. 9434, p 94340G. https://doi.org/10.1117/12.2084996.

(60) Park, S.; Baker, J. O.; Himmel, M. E.; Parilla, P. A.; Johnson, D. K. Cellulose Crystallinity Index: Measurement Techniques and Their Impact on Interpreting Cellulase Performance. *Biotechnol. Biofuels* **2010**, *3* (1), 10. https://doi.org/10.1186/1754-6834-3-10.

(61) Bernstein, J. *Polymorphism in Molecular Crystals*; Oxford University Press, 2007. https://doi.org/10.1093/acprof:oso/9780199236565.001.0001.

(62) Hindi, S. S. Z. The Interconvertiblity of Cellulose's Allomorphs. *Int. J. Innov. Res. Sci. Eng. Technol.* **2017**, *6* (1), 715–722. https://doi.org/10.15680/IJIRSET.2017.0601125.

(63) Meyer, K. H.; Misch, L. Positions Des Atomes Dans Le Nouveau Modèle Spatial de La Cellulose. *Helv. Chim. Acta* **1937**, *20* (1), 232–244. https://doi.org/10.1002/hlca.19370200134.

(64) Zugenmaier, P. *Crystalline Cellulose and Derivatives*; Springer Series in Wood Science; Springer Berlin Heidelberg: Berlin, Heidelberg, 2008. https://doi.org/10.1007/978-3-540-73934-0.

(65) Nishiyama, Y.; Sugiyama, J.; Chanzy, H.; Langan, P. Crystal Structure and Hydrogen Bonding System in Cellulose Iα from Synchrotron X-Ray and Neutron Fiber Diffraction. *J. Am. Chem. Soc.* **2003**, *125* (47), 14300–14306. https://doi.org/10.1021/ja037055w.

(66) Nishiyama, Y.; Langan, P.; Chanzy, H. Crystal Structure and Hydrogen-Bonding System in Cellulose Iβ from Synchrotron X-Ray and Neutron Fiber Diffraction. *J. Am. Chem. Soc.* **2002**, *124* (31), 9074–9082. https://doi.org/10.1021/ja0257319.

(67) Nishiyama, Y.; Johnson, G. P.; French, A. D.; Forsyth, V. T.; Langan, P. Neutron Crystallography, Molecular Dynamics, and Quantum Mechanics Studies of the Nature of Hydrogen Bonding in Cellulose Iβ. *Biomacromolecules* **2008**, *9* (11), 3133–3140. https://doi.org/10.1021/bm800726v.

(68) Ling, S.; Kaplan, D. L.; Buehler, M. J. Nanofibrils in Nature and Materials Engineering. *Nat. Rev. Mater.* **2018**, *3* (4), 18016. https://doi.org/10.1038/natrevmats.2018.16.

(69) Trache, D.; Hussin, M. H.; Haafiz, M. K. M.; Thakur, V. K. Recent Progress in Cellulose Nanocrystals: Sources and Production. *Nanoscale* **2017**, *9* (5), 1763–1786. https://doi.org/10.1039/C6NR09494E.

(70) Plackett, D.; Letchford, K.; Jackson, J.; Burt, H. A Review of Nanocellulose as a

Novel Vehicle for Drug Delivery. *Nord. Pulp Pap. Res. J.* **2014**, *29* (1), 105–118. https://doi.org/10.3183/npprj-2014-29-01-p105-118.

(71) Kargarzadeh, H.; Mariano, M.; Gopakumar, D.; Ahmad, I.; Thomas, S.; Dufresne, A.; Huang, J.; Lin, N. Advances in Cellulose Nanomaterials. *Cellulose* **2018**, *25* (4), 2151–2189. https://doi.org/10.1007/s10570-018-1723-5.

(72) Palantöken, S.; Bethke, K.; Zivanovic, V.; Kalinka, G.; Kneipp, J.; Rademann, K. Cellulose Hydrogels Physically Crosslinked by Glycine: Synthesis, Characterization, Thermal and Mechanical Properties. *J. Appl. Polym. Sci.* **2020**, *137* (7), 48380. https://doi.org/10.1002/app.48380.

(73) Yang, J.; Medronho, B.; Lindman, B.; Norgren, M. Simple One Pot Preparation of Chemical Hydrogels from Cellulose Dissolved in Cold LiOH/Urea. *Polymers (Basel).* **2020**, *12* (2), 373. https://doi.org/10.3390/polym12020373.

(74) Wang, D. M.; Hao, G.; Shi, Q. H.; Sun, Y. Fabrication and Characterization of Superporous Cellulose Bead for High-Speed Protein Chromatography. *J. Chromatogr. A* **2007**, *1146* (1), 32–40. https://doi.org/10.1016/j.chroma.2007.01.089.

(75) Drozd, R.; Szymańska, M.; Rakoczy, R.; Junka, A.; Szymczyk, P.; Fijałkowski, K. Functionalized Magnetic Bacterial Cellulose Beads as Carrier for Lecitase® Ultra Immobilization. *Appl. Biochem. Biotechnol.* **2019**, *187* (1), 176–193. https://doi.org/10.1007/s12010-018-2816-1.

(76) Li, Y.; Wang, J.; Liu, X.; Zhang, S. Towards a Molecular Understanding of Cellulose Dissolution in Ionic Liquids: Anion/Cation Effect, Synergistic Mechanism and Physicochemical Aspects. *Chem. Sci.* **2018**, *9* (17), 4027–4043. https://doi.org/10.1039/C7SC05392D.

(77) El Achkar, T.; Fourmentin, S.; Greige-Gerges, H. Deep Eutectic Solvents: An Overview on Their Interactions with Water and Biochemical Compounds. *J. Mol. Liq.* **2019**, *288*, 111028. https://doi.org/10.1016/j.molliq.2019.111028.

(78) Wang, H.; Gurau, G.; Rogers, R. D. Ionic Liquid Processing of Cellulose. *Chem. Soc. Rev.* **2012**, *41* (4), 1519–1537. https://doi.org/10.1039/c2cs15311d.

(79) Zhang, J.; Wu, J.; Yu, J.; Zhang, X.; He, J.; Zhang, J. Application of Ionic Liquids for Dissolving Cellulose and Fabricating Cellulose-Based Materials: State of the Art and Future Trends. *Mater. Chem. Front.* **2017**, *1* (7), 1273–1290. https://doi.org/10.1039/c6qm00348f.

(80) Moohan, J.; Stewart, S. A.; Espinosa, E.; Rosal, A.; Rodríguez, A.; Larrañeta, E.;

Donnelly, R. F.; Domínguez-Robles, J. Cellulose Nanofibers and Other Biopolymers for Biomedical Applications. A Review. *Appl. Sci.* **2019**, *10* (1), 65. https://doi.org/10.3390/app10010065.

(81) Hu, H.; Yuan, W.; Liu, F.-S.; Cheng, G.; Xu, F.-J.; Ma, J. Redox-Responsive Polycation-Functionalized Cotton Cellulose Nanocrystals for Effective Cancer Treatment. *ACS Appl. Mater. Interfaces* **2015**, *7* (16), 8942–8951. https://doi.org/10.1021/acsami.5b02432.

(82) Löbmann, K.; Svagan, A. J. Cellulose Nanofibers as Excipient for the Delivery of Poorly Soluble Drugs. *Int. J. Pharm.* **2017**, *533* (1), 285–297. https://doi.org/10.1016/j.ijpharm.2017.09.064.

(83) Löbmann, K.; Wohlert, J.; Müllertz, A.; Wågberg, L.; Svagan, A. J. Cellulose Nanopaper and Nanofoam for Patient-Tailored Drug Delivery. *Adv. Mater. Interfaces* **2017**, *4* (9), 1600655. https://doi.org/10.1002/admi.201600655.

(84) Gericke, M.; Trygg, J.; Fardim, P. Functional Cellulose Beads: Preparation, Characterization, and Applications. *Chem. Rev.* **2013**, *113* (7), 4812–4836. https://doi.org/10.1021/cr300242j.

(85) Sen, S.; Martin, J. D.; Argyropoulos, D. S. Review of Cellulose Non-Derivatizing Solvent Interactions with Emphasis on Activity in Inorganic Molten Salt Hydrates. *ACS Sustain. Chem. Eng.* **2013**, *1* (8), 858–870. https://doi.org/10.1021/sc400085a.

(86) Heinze, T.; Koschella, A. Solvents Applied in the Field of Cellulose Chemistry: A Mini Review. *Polímeros* **2005**, *15* (2), 84–90. https://doi.org/10.1590/S0104-14282005000200005.

(87) Tulos, N.; Harbottle, D.; Hebden, A.; Goswami, P.; Blackburn, R. S. Kinetic Analysis of Cellulose Acetate/Cellulose II Hybrid Fiber Formation by Alkaline Hydrolysis. *ACS Omega* **2019**, *4* (3), 4936–4942. https://doi.org/10.1021/acsomega.9b00159.

(88) Wang, G.; Li, F.; Li, L.; Zhao, J.; Ruan, X.; Ding, W.; Cai, J.; Lu, A.; Pei, Y. *In situ* Synthesis of Ag-Fe3O4 Nanoparticles Immobilized on Pure Cellulose Microspheres as Recyclable and Biodegradable Catalysts. *ACS Omega* **2020**, *5* (15), 8839–8846. https://doi.org/10.1021/acsomega.0c00437.

(89) Wu, H.; Tian, H. F.; Li, S. J.; Wang, Y. T.; Ma, Z. C.; Song, Z. H.; Wang, J. G. Preparation, Characterization and Long-Term Antibacterial Activity of Nisin Anchored Magnetic Cellulose Beads. *Cellulose* **2020**, *27* (1), 357–367.

https://doi.org/10.1007/s10570-019-02788-0.

(90) Trygg, J.; Yildir, E.; Kolakovic, R.; Sandler, N.; Fardim, P. Solid-State Properties and Controlled Release of Ranitidine Hydrochloride from Tailored Oxidised Cellulose Beads. *Macromol. Mater. Eng.* **2015**, *300* (2), 210–217. https://doi.org/10.1002/mame.201400175.

(91) Voon, L. K.; Pang, S. C.; Chin, S. F. Porous Cellulose Beads Fabricated from Regenerated Cellulose as Potential Drug Delivery Carriers. *J. Chem.* **2017**, *2017*. https://doi.org/10.1155/2017/1943432.

(92) Mystek, K.; Reid, M. S.; Larsson, P. A.; Wågberg, L. *In situ* Modification of Regenerated Cellulose Beads: Creating All-Cellulose Composites. *Ind. Eng. Chem. Res.* **2020**, *59* (7), 2968–2976. https://doi.org/10.1021/acs.iecr.9b06273.

(93) Zhang, M.; Guo, W.; Ren, M.; Ren, X. Fabrication of Porous Cellulose Microspheres with Controllable Structures by Microfluidic and Flash Freezing Method. *Mater. Lett.* **2020**, *262*, 127193. https://doi.org/10.1016/j.matlet.2019.127193.

(94) Yu, J.; Huang, T. R.; Lim, Z. H.; Luo, R.; Pasula, R. R.; Liao, L. De; Lim, S.; Chen, C. H. Production of Hollow Bacterial Cellulose Microspheres Using Microfluidics to Form an Injectable Porous Scaffold for Wound Healing. *Adv. Healthc. Mater.* **2016**, *5* (23), 2983–2992. https://doi.org/10.1002/adhm.201600898.

(95) Lin, Q.; Gao, M.; Chang, J.; Ma, H. Highly Effective Adsorption Performance of Carboxymethyl Cellulose Microspheres Crosslinked with Epichlorohydrin. *J. Appl. Polym. Sci.* **2017**, *134* (2), 1–11. https://doi.org/10.1002/app.44363.

(96) Metaxa, A.-F.; Efthimiadou, E. K.; Boukos, N.; Fragogeorgi, E. A.; Loudos, G.; Kordas, G. Hollow Microspheres Based on – Folic Acid Modified – Hydroxypropyl Cellulose and Synthetic Multi-Responsive Bio-Copolymer for Targeted Cancer Therapy: Controlled Release of Daunorubicin, *in vitro* and *in vivo* Studies. *J. Colloid Interface Sci.* **2014**, *435*, 171–181. https://doi.org/10.1016/j.jcis.2014.08.001.

(97) Singh, P.; Duarte, H.; Alves, L.; Antunes, F.; Le Moigne, N.; Dormanns, J.; Duchemin, B.; Staiger, M. P.; Medronho, B. From Cellulose Dissolution and Regeneration to Added Value Applications — Synergism Between Molecular Understanding and Material Development. In *Cellulose - Fundamental Aspects and Current Trends*; InTech, 2015; p 13. https://doi.org/10.5772/61402.

(98) Wondraczek, H.; Petzold-Welcke, K.; Fardim, P.; Heinze, T. Nanoparticles from Conventional Cellulose Esters: Evaluation of Preparation Methods. *Cellulose* **2013**, *20* (2), 751–760. https://doi.org/10.1007/s10570-013-9874-x.

(99) Liu, H.; Hsieh, Y.-L. Ultrafine Fibrous Cellulose Membranes from Electrospinning of Cellulose Acetate. *J. Polym. Sci. Part B Polym. Phys.* **2002**, *40* (18), 2119–2129. https://doi.org/10.1002/polb.10261.

(100) Pinto, R. J. B.; Marques, P. A. A. P.; Martins, M. A.; Neto, C. P.; Trindade, T. Electrostatic Assembly and Growth of Gold Nanoparticles in Cellulosic Fibres. *J. Colloid Interface Sci.* **2007**, *312* (2), 506–512. https://doi.org/10.1016/j.jcis.2007.03.043.

(101) Twentyman, P.; Luscombe, M. A Study of Some Variables in a Tetrazolium Dye (MTT) Based Assay for Cell Growth and Chemosensitivity. *Br. J. Cancer* **1987**, *56* (3), 279–285. https://doi.org/10.1038/bjc.1987.190.

(102) Melancon, M. P.; Lu, W.; Yang, Z.; Zhang, R.; Cheng, Z.; Elliot, A. M.; Stafford, J.; Olson, T.; Zhang, J. Z.; Li, C. *In vitro* and *in vivo* Targeting of Hollow Gold Nanoshells Directed at Epidermal Growth Factor Receptor for Photothermal Ablation Therapy. *Mol. Cancer Ther.* **2008**, *7* (6), 1730–1739. https://doi.org/10.1158/1535-7163.MCT-08-0016.

(103) Wsoo, M. A.; Shahir, S.; Mohd Bohari, S. P.; Nayan, N. H. M.; Razak, S. I. A. A Review on the Properties of Electrospun Cellulose Acetate and Its Application in Drug Delivery Systems: A New Perspective. *Carbohydr. Res.* **2020**, *491* (January), 107978. https://doi.org/10.1016/j.carres.2020.107978.

(104) Fei, P.; Liao, L.; Cheng, B.; Song, J. Quantitative Analysis of Cellulose Acetate with a High Degree of Substitution by FTIR and Its Application. *Anal. Methods* **2017**, *9* (43), 6194–6201. https://doi.org/10.1039/C7AY02165H.

(105) Van Rie, J.; Thielemans, W. Cellulose-Gold Nanoparticle Hybrid Materials. *Nanoscale* **2017**, *9* (25), 8525–8554. https://doi.org/10.1039/c7nr00400a.

(106) Huang, X.; El-Sayed, M. A. Gold Nanoparticles: Optical Properties and Implementations in Cancer Diagnosis and Photothermal Therapy. *J. Adv. Res.* **2010**, *1* (1), 13–28. https://doi.org/10.1016/j.jare.2010.02.002.

(107) Link, S.; El-Sayed, M. A. Size and Temperature Dependence of the Plasmon Absorption of Colloidal Gold Nanoparticles. *J. Phys. Chem. B* **1999**, *103* (21), 4212–4217. https://doi.org/10.1021/jp984796o.

(108) Sánchez-Moreno, P.; de Vicente, J.; Nardecchia, S.; Marchal, J.; Boulaiz, H.

Thermo-Sensitive Nanomaterials: Recent Advance in Synthesis and Biomedical Applications. *Nanomaterials* **2018**, *8* (11), 935. https://doi.org/10.3390/nano8110935.

(109) Singh, P.; Pandit, S.; Mokkapati, V. R. S. S.; Garg, A.; Ravikumar, V.; Mijakovic, I. Gold Nanoparticles in Diagnostics and Therapeutics for Human Cancer. *Int. J. Mol. Sci.* **2018**, *19* (7), 1979. https://doi.org/10.3390/ijms19071979.

(110) Pitsillides, C. M.; Joe, E. K.; Wei, X.; Anderson, R. R.; Lin, C. P. Selective Cell Targeting with Light-Absorbing Microparticles and Nanoparticles. *Biophys. J.* **2003**, *84* (6), 4023–4032. https://doi.org/10.1016/S0006-3495(03)75128-5.

(111) Chithrani, D. B.; Jelveh, S.; Jalali, F.; van Prooijen, M.; Allen, C.; Bristow, R. G.; Hill, R. P.; Jaffray, D. A. Gold Nanoparticles as Radiation Sensitizers in Cancer Therapy. *Radiat. Res.* **2010**, *173* (6), 719. https://doi.org/10.1667/RR1984.1.

(112) Jain, S.; Hirst, D. G.; O'Sullivan, J. M. Gold Nanoparticles as Novel Agents for Cancer Therapy. *Br. J. Radiol.* **2012**, *85* (1010), 101–113. https://doi.org/10.1259/bjr/59448833.

(113) Majoinen, J.; Hassinen, J.; Haataja, J. S.; Rekola, H. T.; Kontturi, E.; Kostiainen, M. A.; Ras, R. H. A.; Törmä, P.; Ikkala, O. Chiral Plasmonics Using Twisting along Cellulose Nanocrystals as a Template for Gold Nanoparticles. *Adv. Mater.* **2016**, *28* (26), 5262–5267. https://doi.org/10.1002/adma.201600940.

(114) He, H.; Chen, R.; Zhang, L.; Shen, W. Growth of Gold Nanoparticles on Cellulose Nanofibers. *Cellulose* **2020**, *27* (9), 5041–5053. https://doi.org/10.1007/s10570-020-03142-5.

(115) Nakanishi, K.; Tomita, M.; Masuda, Y.; Kato, K. Gold Nanoparticle–Mesoporous Silica Sheet Composites with Enhanced Antibody Adsorption Capacity. *New J. Chem.* **2015**, *39* (5), 4070–4077. https://doi.org/10.1039/C5NJ00033E.

(116) Singh, R.; Lillard, J. W. Nanoparticle-Based Targeted Drug Delivery. *Exp. Mol. Pathol.* **2009**, *86* (3), 215–223. https://doi.org/10.1016/j.yexmp.2008.12.004.

(117) Mitchell, M. J.; Billingsley, M. M.; Haley, R. M.; Wechsler, M. E.; Peppas, N. A.; Langer, R. Engineering Precision Nanoparticles for Drug Delivery. *Nat. Rev. Drug Discov.* **2020**. https://doi.org/10.1038/s41573-020-0090-8.

(118) Chenthamara, D.; Subramaniam, S.; Ramakrishnan, S. G.; Krishnaswamy, S.;

Essa, M. M.; Lin, F.-H.; Qoronfleh, M. W. Therapeutic Efficacy of Nanoparticles and Routes of Administration. *Biomater. Res.* **2019**, *23* (1), 20. https://doi.org/10.1186/s40824-019-0166-x.

(119) Morales-Cruz, M.; Delgado, Y.; Castillo, B.; Figueroa, C. M.; Molina, A.; Torres, A.; Milian, M.; Griebenow, K. Smart Targeting To Improve Cancer Therapeutics. *Drug Des. Devel. Ther.* **2019**, *Volume 13*, 3753–3772. https://doi.org/10.2147/DDDT.S219489.

(120) Lu, P.-H.; Li, H.-J.; Chang, H.-H.; Wu, N.-L.; Hung, C.-F. Gold Nanoparticles Induce Cell Death and Suppress Migration of Melanoma Cells. *J. Nanoparticle Res.* **2017**, *19* (10), 342. https://doi.org/10.1007/s11051-017-4036-y.

(121) ISO 10993-5:2009(E). Biological Evaluation of Medical Devices - Part 5: Tests for *in vitro* Cytotoxicity. **2009**.

(122) Foster, E. J.; Moon, R. J.; Agarwal, U. P.; Bortner, M. J.; Bras, J.; Camarero-Espinosa, S.; Chan, K. J.; Clift, M. J. D.; Cranston, E. D.; Eichhorn, S. J.; Fox, D. M.; Hamad, W. Y.; Heux, L.; Jean, B.; Korey, M.; Nieh, W.; Ong, K. J.; Reid, M. S.; Renneckar, S.; Roberts, R.; Shatkin, J. A.; Simonsen, J.; Stinson-Bagby, K.; Wanasekara, N.; Youngblood, J. Current Characterization Methods for Cellulose Nanomaterials. *Chem. Soc. Rev.* **2018**, *47* (8), 2609–2679. https://doi.org/10.1039/C6CS00895J.

(123) Bittleman, K. R.; Dong, S.; Roman, M.; Lee, Y. W. Folic Acid-Conjugated Cellulose Nanocrystals Show High Folate-Receptor Binding Affinity and Uptake by KB and Breast Cancer Cells. *ACS Omega* **2018**, *3* (10), 13952–13959. https://doi.org/10.1021/acsomega.8b01619.

(124) Park, J.-E.; Kim, M.; Hwang, J.-H.; Nam, J.-M. Golden Opportunities: Plasmonic Gold Nanostructures for Biomedical Applications Based on the Second Near-Infrared Window. *Small Methods* **2017**, *1* (3), 1600032. https://doi.org/10.1002/smtd.201600032.

(125) Wang, H.; Hou, L.; Li, H.; Wang, X.; Cao, Y.; Zhang, B.; Wang, J.; Wei, S.; Dang, H.; Ran, H. A Nanosystem Loaded with Perfluorohexane and Rose Bengal Coupled Upconversion Nanoparticles for Multimodal Imaging and Synergetic Chemo-Photodynamic Therapy of Cancer. *Biomater. Sci.* **2020**, *8* (9), 2488–2506. https://doi.org/10.1039/C9BM02081K.

(126) Wang, S.; Liu, K.; Wang, F.; Peng, F.; Tu, Y. The Application of Micro- and Nanomotors in Classified Drug Delivery. *Chem. – An Asian J.* **2019**, *14* (14),

2336–2347. https://doi.org/10.1002/asia.201900274.

(127) Yu, Y.; Guo, J.; Zou, M.; Cai, L.; Zhao, Y. Micromotors from Microfluidics. *Chem. - An Asian J.* **2019**, *14* (14), 2417–2430. https://doi.org/10.1002/asia.201900290.

(128) Zarei, M.; Zarei, M. Self-Propelled Micro/Nanomotors for Sensing and Environmental Remediation. *Small* **2018**, *14* (30), 1800912. https://doi.org/10.1002/smll.201800912.

(129) Peng, F.; Men, Y.; Tu, Y.; Chen, Y.; Wilson, D. A. Nanomotor-Based Strategy for Enhanced Penetration across Vasculature Model. *Adv. Funct. Mater.* **2018**, *28* (25), 1706117. https://doi.org/10.1002/adfm.201706117.

(130) Venugopalan, P. L.; Esteban-Fernández de Ávila, B.; Pal, M.; Ghosh, A.; Wang, J. Fantastic Voyage of Nanomotors into the Cell. *ACS Nano* **2020**, *14* (8), 9423–9439. https://doi.org/10.1021/acsnano.0c05217.

(131) Kim, S. M.; Faix, P. H.; Schnitzer, J. E. Overcoming Key Biological Barriers to Cancer Drug Delivery and Efficacy. *J. Control. Release* **2017**, *267*, 15–30. https://doi.org/10.1016/j.jconrel.2017.09.016.

(132) Paxton, W. F.; Kistler, K. C.; Olmeda, C. C.; Sen, A.; St. Angelo, S. K.; Cao, Y.; Mallouk, T. E.; Lammert, P. E.; Crespi, V. H. Catalytic Nanomotors: Autonomous Movement of Striped Nanorods. *J. Am. Chem. Soc.* **2004**, *126* (41), 13424–13431. https://doi.org/10.1021/ja047697z.